The formation of fragments in symmetric heavy ion collisions

P.-B. Gossiaux[1,2] and J. Aichelin[1]

[1] *SUBATECH*

Université de Nantes, EMN, IN2P3/CNRS F-44072 Nantes, France

[2] *Max Planck Institut für Kernphysik, D-Heidelberg, Germany*

Heidelberg, Max Planck Inst.

Abstract

We investigate in detail the fragment observables as well as the formation of fragments in simulations of symmetric reaction between $E_{kin} = 30$ A MeV and 600 A MeV employing the Q.M.D. model. After a comparison with existing data we investigate the double differential cross section $\frac{d\sigma}{dp_z p_t dp_t}$ the variance and the mean values of the rapidity distribution of fragments and the multiplicity distribution. Investigating the production mechanism we find at all energies that those nucleons which are finally in a fragment have strong initial - final state correlations in coordinate as well as in momentum space. At high energy the correlations resembles the participant spectator model, at low energy the correlations are more complicated but equally strong. They are a consequence of the Pauli blocking of the NN collisions, the geometry and the excitation energy. These correlations describes which nucleons have a higher change to be finally in a fragment but do not describe in which of the up to 12 fragments. The actual fragments are formed by nucleons which come close together in the course of the reaction but can be initially quite separated in coordinate as well as in momentum space. Fragments can therefore be considered as nucleon correlations caused by the dynamics of the reaction. Finally we discuss the origin of high energetic protons observed also experimentally ("Fermijets") and investigate whether we can confirm that subsystems (like the spectator matter) can be considered as a thermalized, as recently conjectured.

1 Introduction

The multifragmentation of nuclei excited in collisions with protons or heavy ions is one of the most interesting and challenging topics in present-day heavy-ion physics. The production of intermediate mass fragments (IMF), which we define as an object with $3 \leq Z \leq 25$, in collisions of a proton with heavy targets is known since almost 40 years [1]. Using radiochemical methods, however, a total cross section for fragmentation could not be determined and this process has been considered as quite rare and exotic. It took another 30 years before fragmentation gained general interest and was considered as that interesting that special (4π) detectors have been designed to study this process in detail. Today the study of multifragmentation is a major research project at all heavy ion accelerators.

Two findings, one experimental and one theoretical, have placed multifragmentation into the spotlight. Bombarding large target nuclei with heavy ions Warwick at al. [2] found that many IMF's are produced simultaneously and that multifragmentation is the dominant reaction channel at beam energies larger than 35 AMeV. Observing that the mass yield curve obeys approximately a power law $\sigma(A) \propto A^{-\tau}$ the Purdue group [3] conjectured that multifragmentation is a clear signature [4] for the phase transition between a gaseous and a liquid phase of nuclear matter. This transition is predicted to occur around a density of 0.4 ρ_0.

Despite extensive experimental efforts, the underlying physical explanation for why a nucleus disintegrates into many (up to 15) IMF's remains controversial. This is due to the fact that multifragmentation shows many puzzling aspects which we will summarize shortly and almost all models succeed in describing some of them but fail to describe the others.

It is observed that independent of the mass of the projectile-target combination, the *form* of the mass yield curve [5] is almost identical from 30 AMeV up to highest energies although the underlying process changes. At low energy, the whole nucleus takes part in the multifragmentation to the limit that the process can be described as a compound nucleus decay, whereas at high energies, only the spectator part contributes [5]. The same conclusion can also be reached on the basis of the observation that at low energies, the slopes of the energy spectra of protons and IMF's agree, whereas starting from about 100 AMeV, increasingly different slopes are observed [6].

The backward energy spectra of fragments are found to be rather independent of the beam energy [7, 2] and the projectile mass [2] (for $A_{\mathrm{proj}} \leq 20$) and at each angle can be fitted to a Maxwellian form for a finite source ve-

locity. However, the spectra at different angles cannot be described by a moving source fit [2, 6] because one must either assume an angle-dependent Coulomb barrier or an angle-dependent slope of the spectrum [8]. However, the presently available experimental triple differential cross section $d\sigma/dEd\Omega dZ$ at beam energies larger than 50 AMeV leave a lot to be desired and firm quantitative conclusions cannot be drawn. However, the recently performed experiments of the ALADIN/MSU and the FOPI collaborations at SIS as well as of the INDRA collaboration at GANIL will improve the situation quite soon. The energy balance in central collisions is dominated by a large undirected flow component ($\beta \approx 0.1c$) and the Coulomb repulsion and the possible thermal energy represent only a minor part [9]. The slope of the high energy tails of the fragment energy spectra in pA collisions does not agree with the temperature extracted from the isotopic yield [3] despite both distributions having the functional form expected for a completely thermalized system. To make progress towards an understanding of the underlying processes it would be highly desirable to know whether this observation is also valid in heavy ion induced reactions.

The models advanced to describe multifragmentation invoke practically all imaginable physical processes. For a recent review we refer to ref [5]. However, most of the phenomenological models have been superseded in the last years by numerically involved models which predict results for a multitude of observables simultaneously and do not try to concentrate on the explanation of one or the other observation only. Presently two types of this kind of models are discussed.

Firstly, statistical models [10, 11, 12] which neglect all dynamics of the reaction and assume that all possible exit channels (consisting of - possibly excited - fragments and nucleons) are occupied with equal probability during the reaction. They assume that the system or a subsystem reaches equilibrium in the course of the reaction and maintain this equilibrium until the system has reached a density around 0.4 ρ_0. These models have been proven to describe mass yields, fragment multiplicities and fragment mass correlations for 800 AMeV reactions very accurately [14] but are in no way appropriate for a description of the dynamical variables [9, 15]. Since the most accurate mass yield measurements have been performed for peripheral reactions whereas the energy spectra are available mainly for central collisions one can presently - due to the lack of fragment energy spectra for peripheral reactions- not exclude that statistical models have a realm of applicability for large impact parameters. Intuitively, however, one would expect that they are valid, if at all, in central collisions, where due to the

many collisions the system should come easier to equilibrium.

The statistical models, claiming to describe the reaction in the whole range of impact parameters, leave a couple of important questions unanswered: First how can a system appear to be equilibrated to a high degree of accuracy when fragment mass distributions are considered, yet appear to be not at all equilibrated in dynamical variables? Second, what is - under these circumstances - the physical meaning of quantities like temperature, chemical potential or the entropy extracted from mass yield distribution? Taking the latest results [9, 15] seriously, for a wide range of impact parameters and energies thermodynamic quantities can at most be considered as a set of fit parameters. The dynamics of that reaction for which thermodynamics has been applied most successfully we will investigate in detail in section 7.

A second type of approach is the Quantum Molecular Dynamics (Q.M.D.) [16] model which follows the time-evolution of the full multi-nucleon phase space distribution from the initial separation of projectile and target up to the final formation of fragments. This model is even more ambitious than the statistical approach but requires also more approximations. The most severe is the fact that the antisymmetrization of the nuclear wave function cannot be taken into account. Therefore all properties which have to do with shell structures cannot be accounted for.

In the QMD model extensive calculations have been performed for the recent 4 π detector experiments at GSI, MSU and GANIL. The data obtained at these facilities are to a large extend still preliminary but allow the conclusion that starting from 30 AMeV the number of intermediate mass fragments (IMF) as a function of the number of observed charged particles is in quite good agreement with experiment. The comparison between experiment and theory is only made possible by very extended filter programs which determine which of the particles of a numerical simulation would have been detected by the actual apparatus. For this decision a detailed understanding of how the detector reacts to double hits etc. has to be developed. In fig. 1 we present the IMF multiplicity as a function of the number of charged particles N_C obtained by the MSU collaboration [17] for the system Kr + Au at 3 different energies (from 55 AMeV up to 200 AMeV) as compared with filtered QMD calculations. We observe a good agreement between theory and experiment. The same is true if one compares the IMF multiplicity and N_C as a function of the beam energy as presented in fig. 2. A similar agreement as with the MSU data has also be obtained for the recent measurements with the INDRA detector at GANIL (fig. 3). Here the

filter routines are still preliminary.

This good agreement at the lowest beam energy is surprising because at least some of the approximations which have been made in order to derive the QMD equations, are not valid anymore. These approximations include the quasi particle approximation, the neglect of interference effects between subsequent collisions (the particles behave like classical billiard balls) as well as the assumption that the Pauli blocking of scattering into already occupied phase space cells can be properly modeled. Whereas at high beam energies the few artificial collisions due to the imperfect Pauli blocking do not play an important role they become increasingly important at low energies where the number of true collisions decreases rapidly.

At energies, $E > 400AMeV$, the present version of the QMD models fails to describe the multiplicity of the intermediate mass fragments [18] although the number of nucleons bound in clusters is reproduced as a function of the N_C The reason is not understood yet. However, we could demonstrate that this failure is not due to the thermal properties of the QMD nuclei but is related to the low momentum transfer to the spectators [19]. Statistical models models succeed to describe these mass yields [14]. However, they have the freedom to adjust the excitation energy of the system by hand. In the QMD approach the excitation energy is completely determined by the solution of the time evolution equations for the nucleons.

The percentage of nucleons bound in fragments decreases rapidly with increasing energy. The results of QMD calculations for $Z \geq 3$ as compared to the experiments of the FOPI collaboration is presented in fig. 4. The maximum of that curve is obtained for beam energies around 50 A MeV.

In view of the increasing evidence that in the energy range from $30AMeV \geq E \leq 400AMeV$ the QMD model describes the measured data quite well it is worthwhile to investigate the fragmentation mechanism in this model which is the purpose of this article. For performing this analysis we take advantage of the fact that in the QMD model momenta <u>and</u> positions of all nucleons are given from the beginning until the end of the reaction. This allows to address the questions, whether initial-final state correlations play an important role for the multifragmentation, whether the fragments are only formed at the end of the reaction and which is the environment of those nucleons, which are going to form a fragment during the time evolution of the system. The ultimate goal of this investigation is an understanding of the multifragmentation in simple physical terms. In this paper we concentrate on symmetric systems. At low energies we do not expect that asymmetric systems behave very differently. At higher energies, where the geometry

may become more important, there may be differences, i.e. in a asymmetric system the projectile may drill a hole through the target nucleus what has of course consequences for the geometrical structure of the spectator part. This will be investigated in an upcoming publication.

The paper is organized as follows. In the second section we introduce briefly the model and comment the differences between the presently existing QMD programs. In section 3 we give a survey of the reactions investigated which is followed by the investigation of the question whether there is evidence that the system thermalizes as a whole. Section 5 and 6 are devoted to a detailed study of correlations between initial and final state. In section 7 we address finally the question whether thermalized subsystems can be identified. The conclusion of our work is given in section 8.

2 The Model

The main assumption of Q.M.D. is that the total nuclear n body wave function can be taken as a product of gaussian wave functions (one per nucleon, in r and p spaces). The Gaussians have to be considered as test wave functions for a variational approach. This parametrization is very convenient for defining the fragments emerging from the reaction : a simple minimum spanning tree method applied to the centroids of those gaussians permits - almost parameter free - to obtain clusters. This parametrization also allows to introduce the imaginary part of the Brückner G - matrix, i.e. nucleon nucleon collisions, in a straightforward manner. Comparison of TDHF calculations which lack the collisions, with experiments show the importance of NN collisions for the angular distribution of the particles. Another advantage of this parametrization is the possibility to label each nucleons and hence to trace back the nucleons forming the asymptotic fragments in order to investigate their earlier properties. One can thus associate properties to one class of final fragments or, equivalently, explore initial-final state correlations and the formation mechanism.

Recently attempts have been made to include the antisymmetrization of the n - body wave function. However, due to the huge numerical complexity the predictions are limited to systems which are not interesting from the point of view of multifragmentation [20, 21]. How to overcome for large systems the numerical problems due to the N! terms of the Slater determinant as well as how to treat collisions between the nucleons in this approach remains up to now an open problem. The time evolution of the nucleons in

the real part of the Brückner G - matrix is in both approaches calculated by a generalized Ritz variational principle.

The QMD model has been extensively discussed in a recent Physics Reports [16]. Later the results have been updated in another review [22, 23]. Therefore we do not repeat the details here.

However, we would like to comment on some confusion which has recently been reported. Since we introduced the QMD programs ten years ago [24], the program has been further developed by many people, but not all developments are suited as general purpose simulation programs. The first version which allowed quantitative comparisons with data has been used in [25]. The QMD program used in the present calculation is the same as that already used in [16, 27] The results obtained here and in these publications can therefore be compared. This program was especially adjusted to low energy heavy ion reactions by introducing Coulomb trajectories in the entrance channel, by improving the description of the Pauli principle and by optimizing the binding energies of the nuclei. All of these improvements should not have a significant influence on results of high energy heavy ion reactions. In this program there exist the option for a time consuming but more precise higher order Runge Kutta algorithm for the propagation of particles which has been used if energy conservation on the percent level was required [28]

The so called IQMD [29] program solves the same equations but with different numerical techniques. It can be as well considered as a general purpose approach. In distinction to the above mentioned QMD program it has a finite lifetime of the Δ resonance and allows therefore to investigate in detail the pion spectra etc. Also the initialization of projectile and target is done differently. In the QMD program [27, 28] heavy nucleons have initially a Wood Saxon like distribution with a central density of $.145 N/fm^3$ and hence a little bit smaller than predicted by Hartree Fock calculations ($.155 N/fm^3$) [30] whereas the IQMD as well as [25] assume a sphere with a density of $0.17 N/fm^3$. The different initializations cause different values of the directed flow where one has to keep in mind that the flow is not only extremely sensible to modifications which have little influence on other observables but is also very small in absolute quantity.

Together with the group in Tübingen the Skyrme potential as well as the free cross section [31] has been replaced by the real part resp. a function of the imaginary part of the Brückner G - matrix. In this program the bounce off and the stopping can be studied but - due to unsolved stability problems - not the multifragmentation.

Later two independent program versions have been advanced which simulate the uncertainty relation by a so called Pauli potential [32, 33]. Since - as mentioned above - the many body wave function is not antisymmetrized in the course of the reaction phase space cells of the size h^3 can be occupied by more than one particle due to fluctuations although for the mean occupation this is not possible due to the Liouville theorem. If one introduces a potential which depends on the relative momenta and positions of the nucleons one can suppress this overoccupation. The Pauli potential provides well defined nuclear ground states which corresponds to the minimum of the Hamiltonian used in the calculation. The price one has to pay, however, is that although the nucleons in a isolated nucleus carry their proper Fermi momentum, they do not move relative to the center of mass of the nucleus, since $dr_i/dt = 0$. This corresponds to a crystallization of the cold nucleus in phase space: Only a collective motion of the nucleons is possible because if only one nucleon is moved it enters an already occupied phase space cell. Due to this crystallization in a reaction the fragments are excited for a much longer time then in the above mentioned QMD versions in which fragments are practically cold after 180 - 200 fm/c as we will see in section 7. Therefore, at the end of the calculation, a so called afterburner, i.e. a statistical evaporation program has to be employed to deexcite the excited fragments to ground state nuclei. Especially at low energies one cannot expect the QMD with Pauli potential gives the same fragmentation pattern as the standard QMD. Indeed large discrepancies between both versions can be observed if one compares the results in fig. 1 and 2 with that of ref.[34] where a program with Pauli potential has been used.

In this paper we will fully take advantage of the above mentioned backtracing tool. To clarify the way it works, we give a specific example in the following. At high energies ($\gg$ 100 AMeV), a model widely referred in the literature is the participant-spectator model [35]: given two colliding nuclei and their impact parameter, one can define their geometrical overlap. Nucleons in the geometrical overlap volume are called participants, the others spectators. Projectile and target participants can interact directly and produce a hot compressed matter, called fireball, from which nucleons and small clusters escape. On the other hand, in the most simple version of the model spectator nucleons of projectile and target do not take part in the nucleus nucleus collision. In more sophisticated versions some participants interpenetrate the spectator matter and excite it mildly. Thus the spectator matter may finally disintegrate into several IMF's.

Thus this model predicts a clear correlation between the initial state

(here the position in the impact parameter plane) and the final fate of the nucleon (being part of an IMF or a free nucleon). A lot of experimental data have been gathered which can be interpreted in the framework of the participant-spectator model. Hence it is interesting to study whether this phenomenological model can be verified in a dynamical simulation of the reaction as provided by Q.M.D. model.

To show how well those correlations can be obtained in the Q.M.D. model, we shall proceed in the following way:

- store the initial positions $r_i(t = 0)$ and momenta $p_i(t = 0)$ of all $A_P + A_T$ nucleons
- simulate a reaction up to t = 180 fm/c
- perform clusterization at t = 180 fm/c using a minimum spanning tree;
- define $inclass_i = 1$ if at t = 180 fm/c the nucleon i is part of a fragment belonging to the class one wants to investigate.
- project the initial positions $r_i(t = 0)$ on a 2 dimensional grid. Each vector $r_i(t = 0)$ corresponds now to a grid cell k.
- define 2 quantities $\rho_{class,k} = \sum inclass_i$ and $\rho_{tot,k} = \sum 1$ where the sum runs over all nucleons whose coordinate vector falls into the grid cell k
- perform the mean of ρ's on an ensemble of simulations
- display the quantities ρ_{class} and ρ_{class}/ρ_{tot}.

No correlation between initial and final state means $\rho_{class}/\rho_{tot} = const.$ The participant spectator predicts values of ρ_{IMF}/ρ_{tot} close to 1 outside the geometrical overlap and values of ρ_{IMF}/ρ_{tot} close to zero otherwise.

This method at hand we will study now various possible correlations between initial state and final fate of the nucleons. For peripheral as well as for central collisions we study these correlations as a function of the beam energy for symmetric collisions between heavy nuclei.

Before that, we give account here on the conventions taken in this paper:

- the results are displayed in the nucleus nucleus center of mass system

- the beam axis is in z direction, the impact parameter points into the x direction
- the projectile has initially a positive z momentum and is displaced (for non zero impact parameters) in the positive x direction
- A soft equation of state [16] has been used. Consequently, for some observables (i.e. flow), one does not expect to have quantitative agreement with experiment.
- The scattering angle is always lower than 90° in the nucleon nucleon center of mass system.
- Clusters are determined by a minimum spanning tree procedure, i.e. nucleons which have are closer than 3 fm at the end of the simulation are considered as part of a fragment.

3 Survey of the reaction

Fig.5 presents a survey of the investigated central reaction. For three reactions we plot from top to bottom the time sequence of the density profile of one single event projected onto the plane defined by impact parameter and beam axis. Each nucleon is marked by a circle of the radius of 2 fm. Hence circles which are overlapping refer to clusters (although the projection may fool a little bit). We see three quite different exit channels. The 400 AMeV collisions show fragments only along the beam axis. These were a part of the spectator matter. At 150 AMeV we find already fragments with p_z values close to zero, coming from midrapidity. The pattern of the emission of particles is almost isotropic. At 50 AMeV we observe distinct projectile and target like fragments as well as midrapidity fragments which are clearly separated in momentum and coordinate space. As we will discuss later the majority of the projectile nucleons which are entrained in fragments have traversed the target and vice versa. This is only possible because the Pauli principle blocks almost all collisions.

4 Does the whole system thermalize?

Already fig. 5 shows qualitatively that the stopping is by far not complete and hence a globally equilibrated system is not formed. This can be quan-

tified by measuring the cross section $d\sigma/dErat$ where Erat is defined as

$$Erat = \frac{\sum p_{trans}^2/2m}{\sum p_z^2/2m}. \tag{1}$$

Equilibration corresponds to Erat = 2. In fig. 6 we present this quantity (calculated with the Q.M.D. model by the FOPI collaboration) as compared with experiment. The reproduction of the results for central collisions (the calculation stopped at b = 7 fm) demonstrates that the excitation energy of the system is properly described in the Q.M.D. model. We would like to mention that the stopping is a complicated interplay between mean field, collisions, and the Pauli blocking and thus far from being easily reproduced. The experimental result shows further that global equilibration is almost never obtained at this energy. For further comparisons performed by the FOPI collaboration we refer to a recent publication [9].

The calculation for lower energies, where data have been taken but are not analyzed yet, is presented in fig. 7. For high Erat values we observe about the same slope as for 150 AMeV. Also here Erat values larger than 1.5 are almost never obtained. In view of the strong Pauli blocking of the collisions this is not astonishing but the thermal form of the single particle spectra gave rise to speculations that the system may be thermalized.

At higher energies the experimental as well - as we will see - the theoretical results suggest that the system can be clearly divided in two subsystems, the spectators and the participants, and a global thermalization is therefore not expected.

The spectra $\frac{d\sigma}{p_t dp_t dp_z}$ is presented in fig. 8 for 400 AMeV and 50 AMeV. For 50 AMeV the proton spectra is indeed not far away from what one expects for an isotropic emission from a thermal source at midrapidity. At 50 AMeV the fragment distribution shows already a forward backward enhancement. The slopes for protons and light ions at midrapidity are not very different, however. The situation is quite different at 400 A MeV. We observe 3 sources of proton emission, the midrapidity fireball and the projectile resp. target remnant. For fragments the midrapidity the midrapidity source is weakened and the spectra is dominated by fragments emitted from projectile and target remnant. The importance of the midrapidity source decreases with the size of the fragment under consideration. The slopes at midrapidity are hence quite dependent on the fragment mass.

Therefore we can draw the conclusion that proton spectra are the least meaningful for addressing the question of thermalization. Due to the many nucleon nucleon collisions which take place they reach quite fast a form

compatible with a thermal spectra. The fragments on the contrary maintain much longer a memory on their initial momenta and are therefore a much more suited probe for the equilibration of the system. We have not found evidence that at any energy the investigated systems come to global equilibrium although very central collisions (which contribute however not significantly to the cross section) may come close.

Of course one can try to overcome this situation by either introducing several thermalized sources or by subtracting so called "preequilibrium" particles from the spectra. In view of the smooth transition between the "preequilibrium" particles and the equilibrium component [36] as well as of the finite particle number in these subsystems the introduction of thermodynamical concepts becomes increasingly closer to a description with a set of fit parameters which have no relation with the thermal properties of the system.

5 Initial State Correlations

5.1 Coordinate Space

We start our analysis with an investigation of possible correlations between the final fate of the particles and their initial position. Fig.9 and 10 display this correlation for those nucleons finally entrained in fragments $A > 4$ (HF) for small and large impact parameters, respectively. Fig. 11 and 12 displays the same correlation for light fragments and singles $A \leq 4$ (LF). The contour lines correspond to $\rho_{HF,k}$ ($\rho_{LF,k}$), the boxes sizes correspond to $\rho_{HF,k}/\rho_{tot,k}$ ($\rho_{LF,k}/\rho_{tot,k}$), k being the grid cell. Both quantities are normalized relative to the grid cell with the largest content.

We start from the high energy (600 AMeV), where we understand the things pretty well, and go down to the lowest energy (50 AMeV) where the situation is less clear. At 600 AMeV we observe, first of all and independent from the impact parameter, what we expect from the participant spectator model: HF's come predominantly from the spectator regions whereas LF's have their origin in the participant region. Of course the transition between participants and spectators is not as sharp as in the abovementioned model but still quite distinct. A closer look, however, reveals a z dependence of that correlation, not predicted in the participant spectator model. This z dependence is caused by the expanding fireball. When the end of projectile and target arrive, a fireball has been already formed by the participants at the frontage of the nuclei. Due to their high temperature these nucleons

try to disassemble already before the back end of projectile and target has arrived and thus interpenetrate the spectator matter. This leads to a local excitation (with the dimension of a mean free path) with the consequence that the concerned nucleons have a too high temperature to form a fragment finally. In the later sections of this paper we will substantiate this interpretation.

We would like to interpret this finding in view of the dependence of the transverse flow on the mass number of the fragment. The plastic ball collaboration has observed [37] that the directed transverse flow increases as a function of the mass number. We find here that the large fragments (even in central collisions) are made of spectator nucleons. They do not pass a region of high density. Thus the directed transverse flow does not measure properties of the high density zone but the gradient of the potential at its surface. Therefore the flow can measure the high density properties of nuclear matter only to that extend to which these properties can be inferred from the gradient of the potential at the surface of the high density zone. In addition - as we will see later - the flow is partially created by a selection of nucleons which have already at the beginning of the reaction an average transverse momentum. These findings have to be confronted with the recent observation that the strange particle production at that energy takes place in the high density region [23]. Therefore these particles provide a more direct information about the high density zone.

At central collisions the LF's seem not to display the correlations expected from the participant spectator model. However, this is a consequence of our relative normalization. At central collisions we observe only very few fragments thus, independent of any correlation, $\rho_{LF,k}/\rho_{tot,k} = 1 - \rho_{HF,k}/\rho_{tot,k}$ is always large.

After we have investigated in detail the 600 AMeV case, one can pass to the lower energy. We observe a gradual disappearance of the correlations predicted by the participant spectator model. Already at 400 AMeV the correlations are weakened, mainly do to the fact - as we will see later - that we observe now also HF's formed by participants as indicated by the finite box sizes in the participant region. Between 400 AMeV and 150 AMeV the reaction mechanism changes completely. At 150 AMeV we observe almost no spatial correlation anymore as expected if the system equilibrates completely. That this conjecture is not true at all we will see later. At central collisions at 50 AMeV we observe correlations along the beam axis. Nucleons at the back end of projectile and target have a higher probability to form a light fragment or to stay as a nucleon than those at the front end.

As we will discuss later the formation of a dense zone in the overlap region of projectile and target acts as a catapult for those nucleons which are at the back end of projectile and target. These nucleons become accelerated and do not form heavy fragments finally.

We would like to mention that at 50 AMeV and to a lesser degree at 150 AMeV the projectile nucleons which form heavy fragments have traversed the whole target nucleus and vice versa as can be also seen from fig. 5 in clear distinction to the higher energies where the heavy fragments come from the spectator part. Later we will discuss this phenomenon in detail.

In conclusion, we see a complete change of the coordinate space correlations if we decrease the energy from 600 AMeV to 50 AMeV.

It is helpful to define a single numerical quantity reflecting the importance of the correlation to facilitate the comparison between different energies. In the following, we consider

$$C_{LF} = \frac{\sqrt{\overline{\left(\frac{\rho_{LF}}{\rho_{tot}} - \overline{\left(\frac{\rho_{LF}}{\rho_{tot}}\right)}\right)^2}}}{\overline{\left(\frac{\rho_{LF}}{\rho_{tot}}\right)}} \tag{2}$$

as a relevant quantity for the initial correlations. ρ_{LF} is the initial density of nucleons emerging asymptotically as light fragments and ρ_{tot} is the mean density in initial nuclei. $\overline{(...)}$ represents the mean of all cells with $\rho_{tot} \geq max(\rho_{tot})/10$. This condition is set to discard the unphysical fluctuations in the low density regions.

In a similar way, we define C_{HF} as the "correlation number" for heavy fragments production. As $\rho_{LF}, \rho_{HF} \leq \rho_{tot}$, one can establish easily that

$$C_{LF} \leq \sqrt{\overline{\left(\frac{\rho_{LF}}{\rho_{tot}}\right)}^{-1} - 1}, C_{HF} \leq \sqrt{\overline{\left(\frac{\rho_{HF}}{\rho_{tot}}\right)}^{-1} - 1}, \tag{3}$$

pointing to the fact that correlations are intrinsically limited if a large number of nucleons are requested for a given final channel (as a limit, they vanish if all the nucleons are needed). This is for instance the case in the production of LF in central collisions of high energy, as one can see on the top-left panel of figure 11.

Moreover, as $\rho_{LF} + \rho_{HF} = \rho_{tot}$, one has

$$\overline{\left(\frac{\rho_{LF}}{\rho_{tot}}\right)} * C_{LF} = \overline{\left(\frac{\rho_{HF}}{\rho_{tot}}\right)} * C_{HF} \tag{4}$$

and of course

$$\overline{\left(\frac{\rho_{LF}}{\rho_{tot}}\right)} + \overline{\left(\frac{\rho_{HF}}{\rho_{tot}}\right)} = 1 \tag{5}$$

In table 1 we summarize the values of $\overline{\left(\frac{\rho_{LF}}{\rho_{tot}}\right)}$ and $\overline{\left(\frac{\rho_{HF}}{\rho_{tot}}\right)}$ for Au + Au (E=600,400,150 AMeV) and Xe + Sn (E=50 AMeV) reactions. In table 2,

Table 1: $\overline{\left(\frac{\rho_{LF}}{\rho_{tot}}\right)}$ and $\overline{\left(\frac{\rho_{HF}}{\rho_{tot}}\right)}$

Reaction	b<, LF	b<, HF	b>, LF	b>, HF
Au+Au(600AMeV)	93%	7%	55%	45%
Au+Au(400AMeV)	88%	12%	50%	50%
Au+Au(150AMeV)	63%	37%	36%	64%
Xe+Sn(50AMeV)	33%	67%	24%	76%

we summarize the values of C_{LF} and C_{HF} for the same reactions.

Table 2: C^r_{LF} and C^r_{HF}

Reaction	b<, LF	b<, HF	b>, LF	b>, HF
Au+Au(600AMeV)	0.06	0.75	0.48	0.54
Au+Au(400AMeV)	0.05	0.41	0.45	0.43
Au+Au(150AMeV)	0.06	0.09	0.30	0.16
Xe+Sn(50AMeV)	0.29	0.13	0.26	0.08

For central high energy collisions, one obtains a large number of nucleons going to LF's and, according to relation 3), a low value for the correlation number. For all other high energy reactions and fragment classes, strong correlations are present, as one expects from the participant-spectator model. As the energy decreases, the number of nucleons going to HF's increases and accordingly the associated correlations vanish. One should also remark that the impact parameter plays a much less significant role than at high energies. But the most interesting point is the survivance (b>) or even the rise (b<) of correlations in ρ_{LF} for the lowest energy considered. Of course, the number of nucleons emerging as LF is smaller and relation 3) then allows more correlations. But on the other hand, it only allows, it does not

imply. Intuitively one would expect at these low energies a transition in the direction to a compound nucleus reaction which implies a complete mixing of all nucleons and the disappearance of all initial state correlations. This is clearly not observed.

5.2 Momentum space

Correlations between initial momenta of the nucleons and their final fate, i.e. their probability to end up in a cluster are usually not considered as important. Phenomenological models usually assume that there are no such correlations. The Q.M.D. calculations, however, show quite strong correlations. In Fig. 13 - 16 we present these correlations in momentum space in the same way as those in the coordinate space in fig. 9 - 12.

At 600 AMeV we see that the fragments are formed by those nucleons which have a momentum which points away from the collision partner. This finding is independent of the impact parameter but the correlation is stronger in more central collisions. This means that the abovementioned transverse flow is partially not generated during the collisions but a result of a initial state correlation which questions another time the value of the observable "flow" as a messenger of the properties of the high density zone. At lower energy the correlation in x direction is weakened and starting from $E = 150AMeV$ supplemented by a correlation in z direction. This latter correlation is a consequence of the Pauli blocking of the cross section. The larger the relative momentum in a collisions the more probable the scattered nucleons find an empty place in phase space. In addition, nucleons which finally are part of a P/T LF have less collisions than those being finally free. Both effects together are the cause that nucleons with small $\pm p_z$ are more probable part of a fragment than the others. At E = 50 AMeV the Pauli blocking is severe for almost all relative momenta because almost all momenta one can reach (by drawing a circle around the NN center of momentum with the radius of the relative momentum) in a nucleon nucleon collision belong to already occupied phase space cells. Only for those with particularly large values of p_z the phase space opens up.

To obtain a more quantitative comprehension of the importance of the momentum space correlations we define - equivalent to the coordinate space - a "correlation number" for the p space. In table 3, we display the results, with the same conventions as in table 2.

Note that in general the correlations in r and p spaces are of the same order. A refined participant-spectator model could then include those p

Table 3: C^p_{LF} and C^p_{HF}

Reaction	b<, LF	b<, HF	b>, LF	b>, HF
Au+Au(600AMeV)	0.03	0.44	0.28	0.31
Au+Au(400AMeV)	0.05	0.36	0.36	0.34
Au+Au(150AMeV)	0.16	0.26	0.58	0.31
Xe+Sn(50AMeV)	0.3	0.13	0.47	0.15

space correlations that have been found. Looking closer, correlations in r space are larger than those in p space for high energies and smaller at lower energies.

As an intermediate conclusion, we have confirmed the presence of strong initial state - final state correlations. The correlations are of the same order in momentum and in coordinate space. For the HF's they are strongest at the highest energy but remain at lower energy. The situation is opposite for the LF's. The spatial correlations at high energy are in agreement with the expectations from the participant spectator model. After these global features we proceed now by defining different fragment classes.

5.3 Catapult Mechanism at low energy

A while ago it has been observed that the most energetic nucleons appear in the half plane opposite to the impact parameter [13]. This is surprising because these nucleons have to cross the entire nuclear system. To investigate the origin of this process we have triggered for the reaction 50 A MeV on those nucleons which have finally the highest momentum and searched for their initial position and momentum. The result is presented in fig. 17. We observe that the particles with a moderate final momentum come from the participant part whereas the most energetic nucleons come from the back end of the colliding nuclei. While they pass through the nucleus they get accelerated and only later when they have to overcome the nuclear potential they loose momentum. Initially these nucleons are not faster than their fellow nucleons. The reason for this mechanism is like follows: Initially these nucleons being at the surface feel a density less then the normal nuclear matter density. The nucleons are continuously moving and those nucleons which are initially at the surface would be accelerated towards the center independent of the fact whether a heavy ion collision takes place of

not. However normally this nucleons arrive at the other end of the nucleus and are stopped by a force due to the density gradient. However, if a reaction takes place the density remains almost constant until the nucleons have passed the entire reaction partner. At its end they should get decelerated but now the relative momentum between them and the nucleons at the end of the reaction partner have increased. This is due to the fact that those nucleons move in the opposite direction as compared to those of the nucleus from where the traversing particles come from. The force at the surface is not sufficient to stop them anymore, however the fig. 17 shows that the get decelerated. nucleons at the front end get stopped. This mechanism is a consequence of the fact that at low energy, where the beam energy is comparable with the Fermi energy, there is not much of a density increase but rather the system expands.

5.4 Projectile/target like and midrapidity fragments

As mentioned in the introduction, it is one of the crucial question concerning multifragmentation whether the system passes a state of global equilibrium. We have already seen in the preceeding section, that Q.M.D. calculations do not support the conjecture that equilibrium is established in the course of the reaction. Here we pursue this investigation further. A necessary but not sufficient condition for passing a state of global equilibrium is the mixing of projectile and target nucleons. In a thermal scenario we would expect that in the average the fragments contain as many projectile as target nucleons and deviations are only due to fluctuations caused by the finite fragment size. We would expect a binomial distribution around the mean value of .5. Since, as mentioned, Q.M.D. gives about the right number of fragments, it is worthwhile to investigate the composition of these fragments and to study the properties of fragments as a function of the relative ratio of the entrained projectile and target nucleons. We define $NT_i(NP_i)$ as the number of nucleons finally contained in the fragment i which have been initially in the target (projectile) and

$$a_i = \frac{NP_i}{NT_i + NP_i}.$$

Although there is no clear cut in the calculations it seems to be meaningful to separate the fragments into three classes

- target like fragments (TLF) $0 \leq a_i < 0.25$

- projectile like fragments (PLF) $0.75 \leq a_i \leq 1$
- midrapidity fragments (MRF) $0.25 \leq a_i < 0.75$

Of course, in nature, particles are indistinguishable. Attaching such a flag of origin to each particle is therefore not realistic. But, first of all, we know that in the high energy limit, which is well reached at our energies, the transport of quantum numbers of wide ranges of longitudinal momentum is improbable. In neutron proton scattering almost never the scattering angle is larger than 90° in the nucleon nucleon center of mass. To assume similar relation in pp and nn collisions is therefore acceptable. Second, by going to the Wigner density formalism, we can interpret the time evolution of the Schrödinger equation as the flow of the phase space density. This allows to ask the question from which phase space region the matter comes which is finally contained in the fragments. In this context particles serve only as an expedient to calculate this flow of matter. However, one has to keep in mind that the interpretation of the Wigner density as a phase space density has some problems (because the Wigner density is not positive definite).

If the fragments are formed after the systems has passed a fully equilibrated phase we would expect a distribution of a_i according to a binomial law with a mean value of 0.5 and a variance proportional to the inverse square root of the fragment mass. Thus a_i should be sharply peaked around 0.5 for heavy fragments. On the other hand in the participant spectator model in its simplest version we expect a_i to be either 0 or 1. If one allows some interactions between participant and spectator matter we would expect two peaks around a_i slightly higher than $a_i = 0$ and slightly lower than $a_i = 1$.

In figs. 18 - 21 , we present results for Au+Au at 400 AMeV and for Xe+Sn (50 AMeV) for central and semiperipheral reactions. In the upper left panel we display the double differential pseudo yield of fragments as a function of the mass number (A) and of a_i. As the number of produced fragments decrease steeply for large A, we have divided the double differential yield by the total yield for every A (that is why we call it pseudo), so that the boxes are visible at large A. The price we have to pay for this type of plotting is the loss of all information about the absolute mass yield in this plot. In the upper right panel we plot the mass yield (full line). The dashed line represents the mass yield for MRF's, the dashed-dotted line represents that of PLF's and TLF's. In the lower left panel we present the normalized (to the total number of IMF's) fragment multiplicity of fragments ($A \geq 5$)

as a function of a_i. Finally, in the lower right panel the fragment multiplicity distribution for three classes of fragments is presented.

We start our discussion be investigation the high energy reaction. First of all, we observe that independent of the impact parameter the overwhelming majority of fragments is either projectile like or target like. At 600 AMeV we do not find MRF's at all. At 400 AMeV about 20% of the fragments are MRF's in central collisions and less than 1% in peripheral collisions. The form of the mass yield distribution for MRF's and PLF's is almost identical for central collisions and can be described by a power law. This is a remarkable result in view of the different production mechanisms It confirms the conjecture that the mass yield is not very sensitive on the underlying physical process, a conjecture which is almost unavoidable in view of the experimental observation that the mass yield distribution is almost independent of the beam energy and the size of projectile and target. In peripheral collisions the form of the mass yield distribution is different for MRF's and PLF's. We see from the lower right panel that in peripheral reaction in most cases two heavy remnants survive, what explains the V shape form of the mass yield. The large number of IMF's shows that on the average several (about 4) IMF's are produced together with the heavy remnant even in these peripheral reactions. One should stress that the form of the mass yield distribution does not allow the interpretation that the remnant is just the heaviest IMF.

For peripheral collisions at 50 AMeV we see a remarkable small change as compared to that collisions at 400 AMeV. Also here on the average two heavy remnants survive the reaction and about 5 IMF's are produced. The number of MRF's has increased but represents not more than 20% of all fragments produced. The form of the fragment yield, however, is now the same for PLF's and MRF's as observed in central collisions at 400 AMeV. More heavy fragments are produced which fill the valley between IMF's and the remnants. At central collisions about 25% of all fragments are MRF's and the form of their mass yield is now very close to that of the PLF's for almost all values of A. In the majority of cases we do not observe two remnants but one, which is however projectile or target like. The other remnant disassembles. Hence the fluctuations in the mass yield distributions are large. Between 400 AMeV and 50 AMeV the transition is quite smooth.

To exhibit clearly the evolution of mixing with energy, we show in table 4 the number of MRF's divided by the number of P/TLF's for $b = 3fm$ collisions

Table 4: number of MRF's divided by the number of P/TLF's for $b = 3fm$ collisions

Energy\System	Au+Au	Xe+Sn
600 AMeV	0.19	-
400 AMeV	0.37	-
150 AMeV	0.47	-
50 AMeV	0.4	0.33

In summary, we observe very strong correlations between the origin of the particles (projectile or target) and the fragments they belong to. Most of the fragments remain projectile or target like and midrapidity fragments represent only a at most 30% fraction. At the impact parameters investigated in Q.M.D. simulations the reactions do not pass a state of complete equilibrium which would include chemical equilibrium. This statement is independent of the beam energy and the impact parameter. Thus at 50 AMeV we have not entered the realm of the quasi fusion mode. This observation suggest that one investigates the properties of PLF/TLF's and MRF's separately.

Therefore we go back now to the correlations in r and p space and investigate whether the MRF's and the PLF/TLF's display different correlations.

5.5 Coordinate space correlations II

We start the comparison for three energies by extracting $\overline{\left(\frac{\rho_{MRF}}{\rho_{tot}}\right)}$ and $\overline{\left(\frac{\rho_{T/PLF}}{\rho_{tot}}\right)}$ (table 5), and C_{MRF} and $C_{P/TLF}$ (table 6). C_{MRF} and $C_{P/TLF}$ are defined as C_{HF}, but with the proper selection of the type of fragments.

Comparing table 5 with table 1 we observe as already seen that the TLF/PLF's outnumber the MRF's at all energies. However, midrapidity fragments get increasingly important with decreasing energy. The correlations displayed in table 6 show, that due to the dominance of TLF/PLF $C_{TLF/PLF}$ and C_{HF} are rather close. Very astonishing however are the strong correlations of the MRF's. They show the strongest correlation observed so far and - in central collisions - even an increase with decreasing energy.

Let us now investigate the origin of these correlations in detail. In figure 22 we display the coordinate correlations as in figures 9 - 12 for b = 3fm

Table 5: $\overline{\left(\frac{\rho_{MRF}}{\rho_{tot}}\right)}$ and $\overline{\left(\frac{\rho_{T/PLF}}{\rho_{tot}}\right)}$

Reaction	b<, MRF	b<, P/TLF	b>, MRF	b>, P/TLF
Au+Au(400AMeV)	2%	9%	0.2%	51%
Au+Au(150AMeV)	11%	29%	1%	64%
Xe+Sn(50AMeV)	14%	56%	7%	69%

Table 6: C^r_{MRF} and $C^r_{T/PLF}$

Reaction	b<, MRF	b<, P/TLF	b>, MRF	b>, P/TLF
Au+Au(400AMeV)	0.33	0.55	1.07	0.43
Au+Au(150AMeV)	0.28	0.15	0.69	0.17
Xe+Sn(50AMeV)	0.59	0.11	0.75	0.1

collisions between 400 AMeV and 50 AMeV. The peripheral reactions give qualitatively the same correlations. On the left side of each figure we display the correlations of the MRF's on the right side that of PLF's and TLF's.

At 400 AMeV we see that initially the MRF nucleons are in the participant zone, that of TLF/PLF in the spectator zones, however concentrated at the interface between the two zones. This finding demonstrates that these zones are clearly separated, i.e. participant nucleons does not interpenetrate the spectator matter to that extend that the composition is changed considerably. Please observe also here a z dependence already discussed previously. Already at 150 AMeV this distribution, expected in the participant spectator model, has changed completely. The energy is not anymore sufficient to create a fireball of the participants over the whole extension of the participant region. Rather only around the point of impact a hot zone is created, which is weakened along the z axis. The energy density is highest around the impact point and is lower towards larger values of $|z|$. At large $|z|$ there are not sufficient nucleons of either projectile or target to form MRF's. This behaviour is even more pronounced at 50 AMeV, where the nucleons finally entrained in MRF's are very localized.

5.6 Momentum space correlations II

The momentum space correlations are presented in table 7. As in coordinate space we observe strong correlations. Especially the MRF nucleons are highly correlated which is quite astonishing. Consequently, the participants do not really form a fireball, i.e. an equilibrated system in which all initial correlations are destroyed.

Table 7: C^p_{MRF} and $C^p_{TLF/PLF}$

Reaction	b<, MRF	b<, P/TLF	b>, MRF	b>, P/TLF
Au+Au(400AMeV)	0.34	0.51	0.76	0.34
Au+Au(150AMeV)	0.48	0.37	1.02	0.33
Xe+Sn(50AMeV)	0.27	0.15	0.3	0.16

In fig. 23 we present the momentum space correlation separately for MRF and TLF/PLF using the same technique as for fig. 13 - 16. We observe that those nucleons form predominately fragments which have initially small momenta in the nucleus nucleus center of mass system. Please observe that this a completely different correlation than observed for the TLF/PLF's. These fragments are formed by nucleons which have a momentum which points away from the collision partner, as already discussed.

At lower energies this correlation of MRF nucleons does not change, neither in the form nor in the strength. Thus we can conclude that MRF's select those nucleons which had initially little energy in the center of mass. Those which have a higher energy find in collisions a larger open phase space and a higher chance to perform a collision. Collisions provide a large momentum transfer and lowers the probability to find several fellow nucleons with about the same momentum, a necessary environment to form a fragment.

5.7 partial conclusion

Up to now we have investigated the possible presence of correlation between initial position of nucleons in r and p space and their final fate in the Q.M.D. model. It turned out that there are two rather distinct classes of fragments, those which are dominated by nucleons which have been initially either projectile <u>or</u> target nucleon and those which are close to chemical equilibrium.

For both classes we observe strong correlations, however different in their nature. At high energy we recover the participant spectator model, however with strong supplementary correlations in momentum space. At lower energies we observe the transition towards a hot spot around the impact point of projectile and target which is the source of the emission of MRF's. The TLF/PLF are formed by nucleons which have traversed the entire projectile/target. Since the Pauli blocking of collisions is severe at this energies the projectile nucleons can keep their correlations while traversing the target and vice versa.

In table 8 we summarize our present findings concerning the correlations: the first line at each entry is for the large impact parameter, the second for the small impact parameter. $++$ stands for strong correlation along the axis considered, $--$ for strong anticorrelation and the arrow points into the direction of decreasing energy.

Table 8: Correlations

Fragment \ Correl.	$R_\perp$	$R_\parallel$	$P_\perp$	$P_\parallel$
LF	$++ \to -$ $0 \to 0$	$0 \to -$ $0 \to --$	$++ \to +$ $0 \to 0$	$0 \to --$ $0 \to --$
TLF/PLF	$-- \to 0$ $-- \to 0$	$0 \to 0$ $0 \to 0$	$-- \to -$ $-- \to -$	$0 \to 0$ $0 \to 0$
MRF	$++ \to 0$ $+ \to 0$	$0 \to ++$ $0 \to ++$	$++ \to +$ $0 \to 0$	$+ \to +$ $++ \to +$

6 Time Evolution of the reaction

Now that we have examined in detail initial properties related to the nature of the produced fragments, we shall turn to the time dependance of another set of observables, in order to understand better how those fragments emerge from the reaction.

6.1 Mean momenta

For each fragment we define:

- The mean momentum per nucleon

$$\vec{P}(t) = \frac{\sum_{i=1}^{A} \vec{p_i}(t)}{A} \tag{6}$$

where A is the number of nucleons in the fragment and $\vec{p_i}(t)$ the momentum of its ith nucleon at time t

- The mean momentum of those nucleons which have been originally projectile nucleons

$$\vec{P_p}(t) = \frac{\sum_{i=1}^{A_p} \vec{p_i}(t)}{A_p} \tag{7}$$

where A_p is the number of projectile nucleons in the fragment.

- The mean momentum of those nucleons which have been originally target nucleons

$$\vec{P_t}(t) = \frac{\sum_{i=A_p+1}^{A_p+A_t} \vec{p_i}(t)}{A_t} \tag{8}$$

where A_t is the number of target nucleons in the fragment.

Next we average over all fragments of a given class noted by $\overline{(...)}$. For this investigation we concentrate on the two classes, the MRF with $a_i \in [0.5, 0.75]$ and the PLF with $a_i \in [0.75, 1]$. By limiting ourself to this range we avoid that $\overline{P_z(t)}$ is - up to fluctuations - zero due to momentum conservation.

In fig. 24 we display $\overline{P_x(t)}$, $\overline{P_{p\ x}(t)}$ and $\overline{P_{t\ x}(t)}$ as a function of the corresponding average momenta in z -direction, in time steps of 10 fm/c. The initial values are marked by an enlarged symbol. Consecutive time steps are connected by a line. Boxes represent the variance of $\vec{P}$ at final time. From top to bottom we display this information for 400 AMeV Au + Au b = 3fm , 50 AMeV Xe + Sn, b = 3fm and 50 AMeV Xe + Sn, b = 6 fm. On the left hand side we have the MRF's on the right hand side the PLF's

At 400 AMeV we observe that the projectile as well as the target nucleons which are going to be PLF's have a finite momentum in x direction, on the average about 20 MeV/c. This is already an appreciable fraction of the finally observed directed flow. The PLF nucleons are not equilibrated completely after 200 fm/c, however, the connected excitation energy remains small. The MRF's have initially an average transverse momentum of about 0. They gain transverse momentum in the course of the time by interactions with other nucleons. One may conjecture that this is the onset of the

blast wave observed recently in very central collisions [9]. In both cases the fellow nucleons which do not fall into the considered bin cause a repulsive interaction, i.e. the final transverse momentum is larger than the initial.

This is not the case at 50 AMeV. There we observe a strong attractive interaction for PLF's. (At 150 AMeV we have about the balance between attraction and repulsion.) Also here we see an incomplete equilibration along p_x at final time and a strong preselection of the momenta in x direction. However, the interaction with the nucleons of the other classes turns the direction of the momentum in the course of the reaction. Thus finally we observe even a larger flow in negative p_x direction. Here projectile and target rotate around a common axis and we observe the onset of a deep inelastic collisions. The PLF take part in this rotation which means that those fragments are only emitted after this rotation has taken place. The MRF's equilibrate at that energy and reside almost exactly in the center of mass. This is not the case for the light fragments nucleons, which are only partly stopped. As this energy, however, one cannot invoke the participant-spectator model. That incomplete stopping is related to the longitudinal correlations noticed in section 3.2. At the large impact parameter, in the third row, we have almost the same behaviour as in the more central collisions, with larger transverse momenta and surprisingly larger stopping. However, one can see in the figure as well that in the central collision the particles become accelerated by the field in p_z direction before the stopping begins To conclude this subsection, note that we have here demonstrated that fragments with $a_i \in [0.25, 0.75]$ will be found mostly at mid rapidity and those with $a_i \in [0, 0.25]$ ([0.75,1]) mostly close to target (projectile) rapidity. This non trivial but intuitive result justifies the denominations used so far for those classes.

6.2 Radii and densities

In the last subsection we have gained insight in the general time evolution of the IMF's. In this section we are going to quantify this observation. We investigate in detail how the fragment nucleons (that we call from now on prefragment) are influenced by the interaction with those nucleons which are finally not part of the fragments. For this purpose we define several quantities:

- The mean position of the prefragment as

$$\vec{R}(t) = \frac{\sum_{i=1}^{A} \vec{r_i}(t)}{A} \tag{9}$$

where A is the number of nucleons in the fragment and $\vec{r_i}(t)$ the position of its ith nucleon at time t

- $Rad(t)$, the mean radius of the prefragment as

$$Rad(t) = \sqrt{\frac{\sum_{i=1}^{A}(\vec{r_i}(t) - \vec{R}(t))^2}{A}} \tag{10}$$

- $Rad_{\perp}(t)$, the mean normalized transverse radius of the prefragment as

$$Rad_{\perp}(t) = \sqrt{\frac{3}{2}\frac{\sum_{i=1}^{A}(\vec{r}_{i,\perp}(t) - \vec{R}_{\perp}(t))^2}{A}} \tag{11}$$

where $\vec{.}$ $\perp$ suffix refers to the transverse projection of $\vec{.}$. The 3/2 factor permits a direct comparison with Rad and is at the origin of the "normalized" denomination.

- $\rho_{ext}(t)$, the mean density of matter not belonging to the prefragment, at its center of mass as

$$\rho_{ext}(t) \; \alpha \sum_{i=A+1}^{A_{proj}+A_{targ}} e^{-\frac{(\vec{r_i}(t)-\vec{R}(t))^2}{2\rho_0^2}} \tag{12}$$

where the sum runs on all nucleons not belonging to the fragment, hereafter called external nucleons (by opposition with internal nucleons, the members of the fragment). The small value of $2\rho_0^2$ (2.17 fm^2) selects only external nucleons close to $\vec{R}$, without any supplementary condition.

- $\rho_{int}(t)$, the mean density of the prefragment matter at its center of mass as

$$\rho_{int}(t) \; \alpha \sum_{i=1}^{A} e^{-\frac{(\vec{r_i}(t)-\vec{R}(t))^2}{2\rho_0^2}} \tag{13}$$

One has of course

$$\rho(\vec{R}(t), t) = \rho_{ext}(t) + \rho_{int}(t) \tag{14}$$

but one will see that the distinction between internal and external matter is quite fructuous.

As section 5.1 we take the means (designed by $\overline{(...)}$) on all fragments of a given class and on a significant ensemble of Q.M.D. runs. In figs. 25 and 26 we plot the time evolution of these coordinate space variables. From top to bottom we display for b=3 fm (resp. 6 fm) 400 AMeV Au + Au and 50 AMeV Xe + Sn the average value of midrapidity fragments and for 50 AMeV Xe + Sn that of the projectile like fragments. On the left hand side we plot the radius and the transverse radius, on the right hand side densities. Initially we mark with an arrow the expected value if no initial correlation is present, i.e. if the nucleons are taken randomly but in the proper composition (a_i) from projectile and target. The difference between the full arrows and the squares (resp. circles) may be caused by the fact that we have initial-final state correlations already on the one body level, i.e. that the nucleons which finally are entrained in the fragments are not uniformly distributed over the target resp. projectile nucleus. To subtract these correlations we introduce dashed arrows. The dashed arrow marks the expected value under the condition that the nucleons are taken randomly from a one body density distribution of that nucleons which belong to the class under consideration. A difference between the dotted arrow and the squares (resp. circles) means that true many body correlations are present, for example that nucleons which finally belong to a fragment have already been close together in coordinate space initially. A agreement between the dashed arrows and the full arrows indicates that the average value for the considered class of nucleons does not differ from that for all nucleons.

For 400 AMeV there is no correlation in longitudinal direction but a small in transverse direction. MRF's stem to a large extend from the participant region which has a smaller transverse size than the combined system of participants and spectators. If we go down to the lower energy we observe initial correlations also in longitudinal direction as already seen in Fig. 11 and 12. It takes about 30 fm/c for the 400 AMeV reaction and 50 fm/c for the 50 AMeV reaction until the transverse size of the prefragment, i.e. those nucleons which will finally form a fragment, and the longitudinal size are equal. Please note that the radius decreases, the nucleons from the different regions of projectile and target join to form the fragment. This is reflected at the right hand side be an increase of the density of the prefragment which is initially quite low. However, at the center of the prefragment the density of nucleons which are not going to join the fragment is quite high and exceeds well normal nuclear matter density for the 400 AMeV reaction.

This leads immediately to the conclusion that

- the fragment nucleons pass a region of high density
- at that moment the fragment nucleons do contribute less to the density at the center of the fragment than those nucleons which will not be part of the fragment.
- hence a fragment is not an object which stays together from the initial set up of the simulation up to the final detection.

Please note that after 100 fm/c (for 400 AMeV) or 150 fm/c (for the 50 AMeV reaction) no other nucleons beside the prefragment nucleons can be found around the prefragments. At that time the prefragments have separated from each other and can be considered as real fragments which will be identified by the minimum spanning tree.

6.3 $< P_z >$ and Effective Temperatures

We start with defining the following quantities:

- The mean momentum of the external nucleons is given by

$$\vec{P}_{ext}(t) = \frac{\sum_{i=1}^{A_{ext}(t)} \vec{p}_i(t)}{A_{ext}(t)} \tag{15}$$

  where $A_{ext}(t)$ is the number of nucleons not belonging to the fragment and located within 3 fm from the center of mass of the fragment nucleons at time t.

- The mean momentum of the fragment nucleons (cf Eq.5), that we shall call $\vec{P}_{int}(t)$ in this section
- $T_{ext}(t)$, the effective temperature of the external medium, defined as

$$T_{ext}(t) = \frac{\sum_{i=1}^{A_{ext}(t)} (\vec{p}_i(t) - \vec{P}_{ext}(t))^2}{3.m_n.A_{ext}(t)} \tag{16}$$

  where the sum over i is performed on the same nucleons as for $\vec{P}_{ext}(t)$ and m_n is the nucleon mass. Note that $T_{ext}(t)$ is an effective temperature of the environment which agrees with the true temperature only in the case of a maxwellian momentum distribution. However, being the second moment of the momentum distribution it gives in any case a measure for the excitation energy/nucleon.

- $T_{\perp\ ext}(t)$, the effective transverse temperature of the external nucleons, i.e. the second moment of the momentum distribution in transverse direction.

- $T_{int}(t)$, the effective temperature of the prefragment, defined as

$$T_{int}(t) = \frac{\sum_{i=1}^{A}(\vec{p}_i(t) - \vec{P}_{int}(t))^2}{3.m_n.A} \tag{17}$$

  where A is the number of nucleons in the fragment. Again, this quantity is to be considered as a probe of the "internal" kinetic energy.

- $T_{\perp\ int}(t)$, the effective transverse temperature of the prefragment, defined as above by taking only into account the transverse degrees of freedom.

As above, we average over all fragments of a given class and over a significant ensemble of Q.M.D. runs. Note, however, that we restrict ourself to $PLF's \in [0.5, 1]$ to avoid the trivial zero values of the momenta if we take TLF's into account as well. In fig. 27 and 28 we display the average momenta and the temperatures for the same reaction as in in fig.'s 25 and 26 Also in momentum space we observe strong initial-final state correlations.

Independent of the energy the prefragment nucleons have initially a smaller mean momentum in z direction than the others. However, the external nucleons change their momentum very fast. At the point of highest density the external nucleons have already $P_{ext,z} = 0$. The reason is quite simple. In the radius of 3 fm around the center of the prefragment we have now projectile and target nucleons, this was not the case at initial time. Please note that the average momentum of the prefragment does practically not change in the course of time. It passes through the high density zone as if it were not present. This is not completely true, however, as can be seen from the right hand side where we have plotted the variance of the momentum distributions. Let us start the discussion with the external temperatures. The external temperatures show the expected behaviour. When projectile and target nucleons interact the system heats up and the variance of the momentum distribution increases. In an equilibrated system, the transverse and total temperature should be equal. This is definitively not the case in our results, until 40 fm/c for 400 AMeV reaction and until 90 fm/c for 50 AMeV reaction. This lack of external equilibrium is consistent with all the correlations that we have found so far.

Finally the temperature lowers because the system disassembles and - depending of their velocity - the nucleons leave the 3 fm sphere around the moving center of mass of the prefragment. Now only prefragment nucleons are present in this sphere and therefore the external variances are zero. The fragment nucleons show a completely different behaviour. Initially the prefragment nucleons have a lower variance than expected from a random selection of those nucleons. The MRF's have as expected a quite large variance in the beam direction. If we follow the variance we observe in all cases that the variance decreases even before the system expands, a behaviour which contradicts completely our intuition as well as our experience from thermodynamics. In a thermodynamical language: the fragments cool down by giving energy to the already hot environment. It is obvious that these findings do forbid to interpret the second moment as a temperature. To understand what actually is happening one has to interpret this results backwards in time. Finally only those nucleons form clusters which have small relative momenta. Now in the course of the reaction it happens that nucleons are scattered in the vicinity (in phase space) of one nucleon or a cluster of nucleons. With respect to these nucleons the variance of the relative momentum is smaller after the collision than before. If the nucleons does not scatter once more it may - together with those nucleons close in phase space - leave the interaction region and form a cluster. If it scatters once more it will not be entrained in this cluster and hence is not counted for T_{int}. Thus one may conclude:

- Fragments are formed by nucleons which are brought by accident into the same phase space region (this may be a consequence of two body scattering or of the potential interaction for MRF's) Nucleons entrained in fragments have on the average a smaller second moment of their momentum distribution as compared to the average.

- Initial correlations are present. Geometry and relative momenta determine how probably nucleons are scattered out of or into certain momentum space regions.

- Thus fragmentation is a mixture of conserving initial correlations and the build up of new correlations in the course of the interaction.

- Although located at the same place in coordinate space like the surrounding nucleons, the fragment nucleons have a much lower variance of their relative momenta. The fragment formation is hence a fluctuation on the level of the one body phase space distribution.

7 Are there thermalized subsystems?

Above 400 AMeV all the fragments originate from the spectator matter. MRF's are completely negligible. In fig. 29 we display the time evolution of a b = 8 fm Au + Au reaction at 600 A MeV. Clearly there are some midrapidity nucleons and smaller fragments however most of the particles are concentrated around projectile and target remnant.

This poses the question whether the spectator matter can form a subsystem which thermalizes after it has disentangle from the fireball nucleons and whether it is therefore accessible to a thermodynamical treatment. Indeed, statistical models have been quite successful in describing the mass yield distribution measured for this reaction [14].

At 600 A MeV Au + Au (b = 8 fm) we observe that in the average 192 nucleons are entrained in fragments $A > 5$ and 400 for $A > 3$. As can be seen from fig. 29 smaller fragments and nucleons can be much less clearer attached to either projectile or target spectator. Due to the magnitude of possible exit channels it is not possible in the context of Q.M.D. calculations to investigate in detail whether a distribution expected from a statistical model for a finite particle number is realized. However we can verify whether some necessary but not sufficient conditions for thermalization are fulfilled:

- the average velocity of the fragments has to be independent of the fragment mass, i.e. the fragments may come from a common source
- the variance Δ of the rapidity distribution of the fragments and a possible temperature T of the system are connected by

$$\Delta^2 \cdot A \cdot m \;=\; T_{eff}^{dyn}$$

- the excitation energy E in the system is related with the possible temperature by the relations

$$T_{eff}^{ex} = \sqrt{\frac{E}{a}}$$

  where a is the level density parameter of about A / 8. MeV^{-1}. and both values of the temperature have to be the same

In fig.30 we investigate these conditions. We see from top to bottom the mean rapidity and the squared variance of the rapidity distribution of the

fragments as a function of their mass number, as well as the total energy per nucleon as a function of time.

The mean rapidity of the fragments is slightly below the beam rapidity of 0.54. The heavier fragments approach the beam rapidity whereas the lighter ones are slightly below. Hence the first condition is almost fulfilled.

The squared variance Δ^2 of the rapidity distribution is plotted in a double logarithmic graph. In this graph the second condition results in straight line which is indeed observed for the low mass fragments. The slope of the $variance^2$ is however quite close to -2 and hence quite different from the expected -1 dependence. It is , however, in agreement with data [41],although more precise experiments would be certainly of value. The values extracted for T_{eff}^{dyn} are of the order of 15 MeV. This value is compatible with that found experimentally in [40]. This agreement of our calculation with experiment and the disagreement of both with the prediction of the thermal models make any statement about a possible thermalization premature before a detailed analysis of the momentum distribution of the fragments has been performed.

The energy of the system, i.e. the total energy of those nucleons finally be entrained in projectile (resp.) targetlike fragments with $A > 3$ is displayed in the last row. Initially this energy is high due to some projectile nucleons which are going to be part of the targetlike fragments and vice versa. After the projectile spectator has disentangle from the fireball and before the spectator matter is disassembled into fragments we observe about an excitation energy of 3 A MeV. At 130 fm/c the system is completely deexcited and the difference between the observed of - 6.5 A Mev and the value for finite nuclei of - 8 A MeV is due to the relative motion between the fragments. T_{eff}^{ex} is about 4 MeV, in clear difference to the value of T_{eff}^{dy} extracted from the spectrum.

At 50 A MeV the situation is completely different. The spectator matter has slowed down to about half of the beam velocity and the variance of the rapidity distribution as well as the mean rapidity is constant.

8 Conclusions

We have presented extensive studies in the framework of the QMD model to understand the process of multifragmentation in heavy ion induced reactions. We have validated the QMD approach by showing that the presently available data are in an even better agreement with the calculation as ex-

pected in view of some approximations especially at low energy. We found that at all energies correlations in coordinate and momentum space are conserved during the time evolution of the reaction. The probability that nucleons are finally entrained in fragments depends on their initial localisation in phase space. However, the regions of the initial phase space which leads to a high probability to end up in a fragment are quite different for different energies and different impact parameters. At the highest energy investigated we see the well established participant spectator model (however supplemented by strong correlations in momentum space). At the lowest energy we find a situation which resembles more deep inelastic collisions. In between there is a white range of correlations which has been explained in physical terms. Fragments are dominantly formed from either projectile or target nucleons. The number of fragments which have about the same number of nucleons which have been originally projectile or target increases with decreasing energy but remains in the minority.

According to our analysis fragments are form by fluctuation in phase space, i.e. by the fact that initially or during the time evolution of the reaction some nucleons come by change into the same phase space region. If those nucleons do not suffer a hard scattering they emerge with a large probability as a fragment from the reaction zone. The internal "temperature", i.e, the second moment of the momentum distribution of the fragment nucleons is much lower than that of the environment. This means that we are really dealing with fluctuations, i.e. quantities which are not calculable in a one body theory. We find no evidence that the system or part of the system come to equilibrium, nor do we find evidence that clusters are formed at densities which one expects for the spinodal region. The subsystem which is closest to equilibrium are the spectators in peripheral reactions at high energies. There several observables follow the trend one expects for thermodynamics. The key variable, however, the width of the momentum space distribution as a function of the fragment mass, does definitely not follow this trend, in agreement with experiment and is to large in its absolute value to be consistent with the excitation energy.

References

[1] G. Friedländer et al., Phys. Rev.94, 727 (1954)

[2] A. I. Warwick *et al.*, Phys. Rev. C **27**, 1083 (1983).

[3] A. S. Hirsch *et al.*, Phys. Rev. C **29**, 508 (1984).

[4] M.E. Fischer, Physica **3** 255 (1967) and Rep. Prog. Phys. **67**, 255 (1967)

[5] L. G. Moretto and G. J. Wozniak, Annual Reviews of Nuclear and Particle Science, J. D. Jackson, Ed., **43**, 379 (1993).

[6] U. Milkau, GSI Report 91-34 (1991).

[7] W. Trautmann, Proceedings of the International Symposium "Towards a Unified Picture of Nuclear Dynamics", Nikko, Japan, 1991.

[8] J. Aichelin, J. Hüfner and R. Ibarra, Phys. Rev. C **30**, 107 (1984).

[9] S. C. Jeong *et al.*, Phys. Rev. Lett. **72**, 3468 (1994); U. Sodan, Thesis, U. of Heidelberg, 1994 (unpublished).

[10] D. H. E. Gross, Rep. Prog. Phys. **53**, 605 (1990), and references therein.

[11] J. B. Bondorf, R. Donangelo, I. N. Mishustin, C. J. Pethick, H. Schulz, K. Sneppen, Nucl. Phys. **A443**, 321 (1985).

[12] D. Hahn and H. Stöcker Nucl. Phys. **A476**, 717 (1988).

[13] J.P. Bondorf et al. Nucl. Phys. **A 333** (1980) 285

[14] A. S. Botvina *et al.*, GSI 94-36 (1994).

[15] W. C. Hsi *et al.*, preprint MSUNSCL - 930, 1994; M. Begemann Blaich and W. Trautmann, GSI Nachrichten 05 - 94.

[16] J. Aichelin, Phys. Rep. **202**, 233 (1991), and references therein.

[17] B. Tsang, private communication and proceedings of the international workshop XXII on gross properties of nuclei and nuclear excitations, Hirschegg, Austria, 1994, ed. by H. Feldmeier and W. Nörenberg

[18] M. Begemann Blaich et al., Phys. Rev. C **48**, 610 (1993)

[19] M. Begemann Blaich et al., Phys. Lett. **B 298**, 27 (1993)

[20] H. Feldmeier, Nucl. Phys. **A515**, 147 (1990)

[21] A. Ono, H. Horiuchi, T Maruyama, A Ohnishi, Phys. Rev. Lett. bf 68, 2898 (1992) and Prog. Theor. Phys. bf 87 , 1185 (1992)

[22] J. Aichelin, Prog. Nucl Part. Phys. **30**, 191 (1993) PPNPD

[23] C. Hartnack et al. Nucl Phys. **A580**, 643 (1994)

[24] J. Aichelin and H. Stöcker, Phys. Lett. B 176 (1986) 14.

[25] A. Rosenhauer, J. Aichelin, H. Stöcker, and W. Greiner, Journal de Physique C4 (1986) 395. J. Aichelin, A. Rosenhauer, G. ~~Peilert, H.~~ Stöcker, and W. Greiner, Phys. Rev. Lett. 58 (1987) 1926.

PHYSA

G. Peilert, A. Rosenhauer, H. Stöcker, W. Greiner, and J. Aichelin, Mod. Phys. Lett. A 3 (1988) 459. MPLA

J. Aichelin, G. Peilert, A. Bohnet, A. Rosenhauer, H. Stöcker, and W. Greiner, Phys. Rev. C 37 (1988) 2451.

G. Peilert, H. Stöcker, W. Greiner, A. Rosenhauer, A. Bohnet, and J. Aichelin, Phys. Rev. C 39 (1989) 1402.

M. Berenguer, C. Hartnack, G. Peilert, H. Stöcker, W. Greiner, J. Aichelin, and A. Rosenhauer, Journal of Physics G 18 (1992) 655 JPHG3

G. Peilert, H. Stöcker and W. Greiner Rep. Prog. Phys. 57 (1994) 533 RPPHA

[26] A. Bohnet, J. Aichelin, J. Pochodzalla, W. Trautmann. G. Peilert, H. Stöcker, and W. Greiner, Phys. Rev. C 44 (1991) 2111.

[27] J. Aichelin, J. Cugnon, Z. Fraenkel, K. Frankel, C. Gale, M. Gyulassy, D. Keane, C. M. Ko, J. Randrup, A. Rosenhauer, H. Stöcker, G. Welke, and J. Q. Wu, Phys. Rev. Lett. 62 (1989) 1461.

J. Aichelin, C. Hartnack, A. Bohnet, L. Zhuxia, G. Peilert, H. Stöcker, and W. Greiner, Phys. Lett. B 224 (1989) 34.

J. Aichelin,Phys. Rep. 202 (1991) 233. PRPLC

G.J. Kunde, J. Pochodzalla, J. Aichelin, E. Berdermann, B. Berthier, C. Cerruti, C.K. Gelbke, J. Hubele, P. Kreutz, S. Leray, R. Lucas, U. Lynen, U. Milkau, W.F.J. Müller, C. Ngô, C.H. Pinkenburg, G. Raciti, H. Sann, and W. Trautmann, Phys. Lett. B 272 (1991) 202

W. Müller, M. Begemann-Blaich, and J. Aichelin Phys. Lett. B 298 (1993) 27.

J. Aichelin Prog. Part. Nucl. Phys. Vol.30 (1993) 191

M. Begemann-Blaich, W.F.J. Müller, J. Aichelin, J.C. Adloff, P. Bouissou, J. Hubele, G. Imme, I. Iori, P. Kreutz, GF.J. Kunde, S. Leray, V.

Lindenstruth, Z. Liu, U. Lynen, R.J. Meijer, U Milkau, A. Moroni, C. Ngo, C.A. Oglivie, J. Pochodzalla, G. Racati, G. Rudolf, H. Sann, A. Schüttauf, W. Seidel, L. Stuttge, W. Trautmann, A. Tucholski Phys. Rev. C48 (1993) 610

P.-B. Gossiaux, D. Keane, S. Wang and J.Aichelin Phys. Rev. C (accepted)

C. Dorso and J.Aichelin Phys. Lett. (accepted)

[28] J. Jänicke and J. Aichelin, Phys. Lett. B 256 (1991) 341.

J. Aichelin and J. Jaenicke, Proceedings of the international workshop "Mesons" , Krakau, May 1991, ed. E. Maguyra, World Scientific, Singapore.

J. Jänicke and J. Aichelin,Nucl. Phys. A 547 (1992) 542

C. Hartnack, J. Aichelin, H. Stöcker and W. Greiner Nucl. Phys. A (accepted)

[29] C. Hartnack, J. Aichelin, H. Stöcker, and W. Greiner, Mod. Phys. Lett. A9 (1994) 1151 .

[30] D. Vautherin and D.M. Brink Phys. Rev C5 (1972) 626

[31] A. Bohnet, N. Ohtsuka, J. Aichelin, R. Linden, and A. Fässler, Nucl. Phys. A 494 (1989) 349.

J. Jaenicke, J. Aichelin, N. Ohtsuka, R. Linden, and A. Fässler, Nucl. Phys. A 536 (1992) 201

[32] G. Peilert et al., Phys. Rev. C46 (1992) 1457 G. Peilert et al, Phys. Lett. B 260 (1991) 271

[33] J. Konopka, Prog. Part and Nucl. Physics, 30 (1993) 301

[34] G.F. Peaslee et al., Phys. Rev. C49 (1994) R2271

[35] G. Westfall, J. Gosset, P.J. Johanson, A.M. Poskanzer W.G. Meyer, H.H Gutbrod, A. Sandoval and R. Stock, Phys. Rev. Lett. 37 (1976) 1202.

[36] J. Aichelin, Phys. Rev. C33 (1986) 537

[37] K.G.R. Doss et al., Phys. Rev. Lett. 59 (1987) 2720

[38] B. Borderie *et al.*, INDRA collaboration, GANIL, private communication, and to be published.

[39] Preliminary data from the EOS detector also support this conclusion.

[40] J. Dreute et al., Phys. Rev. **C44** (1991) 1057

[41] F.P. Brady et al., Phys. Rev. C50 (1994) R525

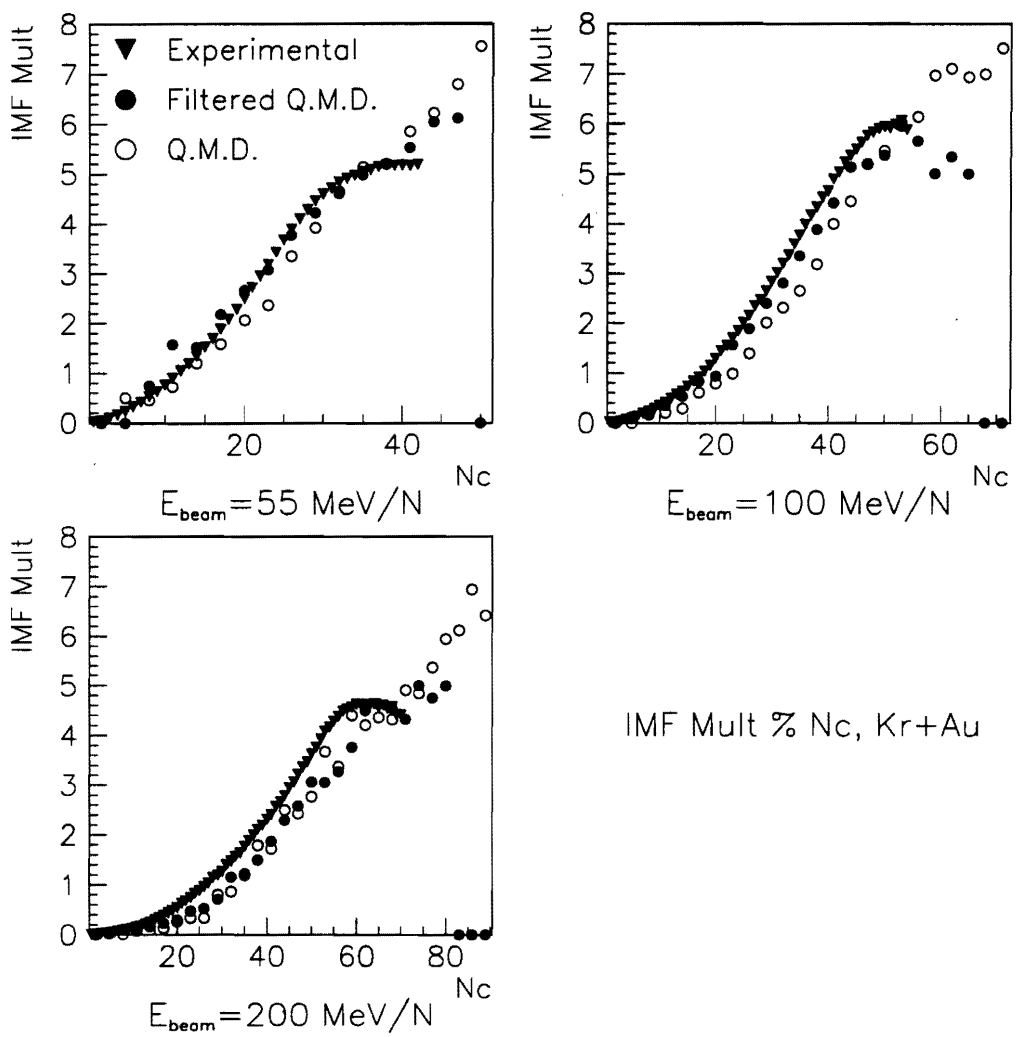

Figure 1: Mean fragment multiplicity as a function of the number of charged particle N_C for Kr + Au at three different energies. We compare the experiment with the filtered Q.M.D. results.

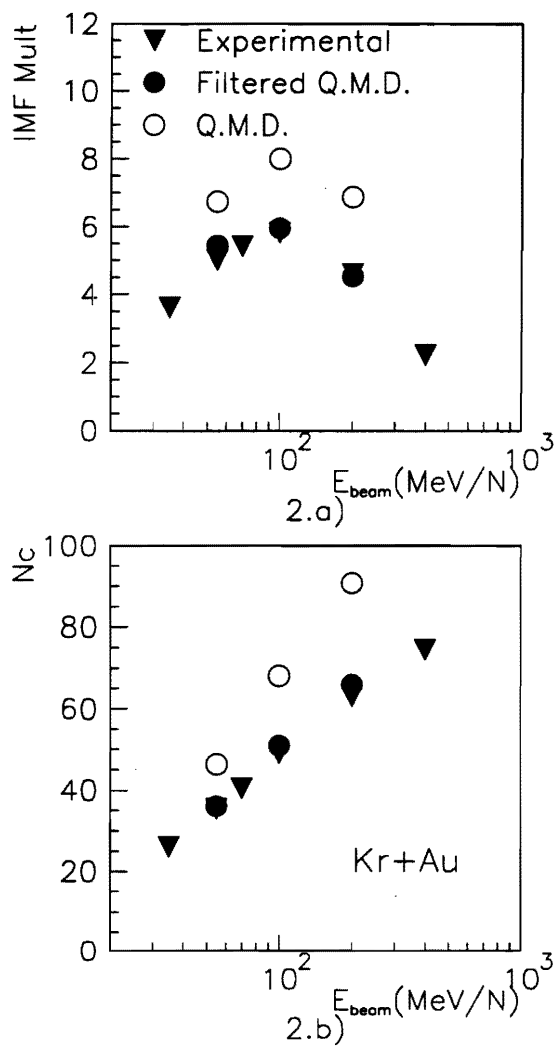

Figure 2: Average number of the intermediate mass fragments and of the charged particles as a function of the beam energy for the reaction Kr + Au

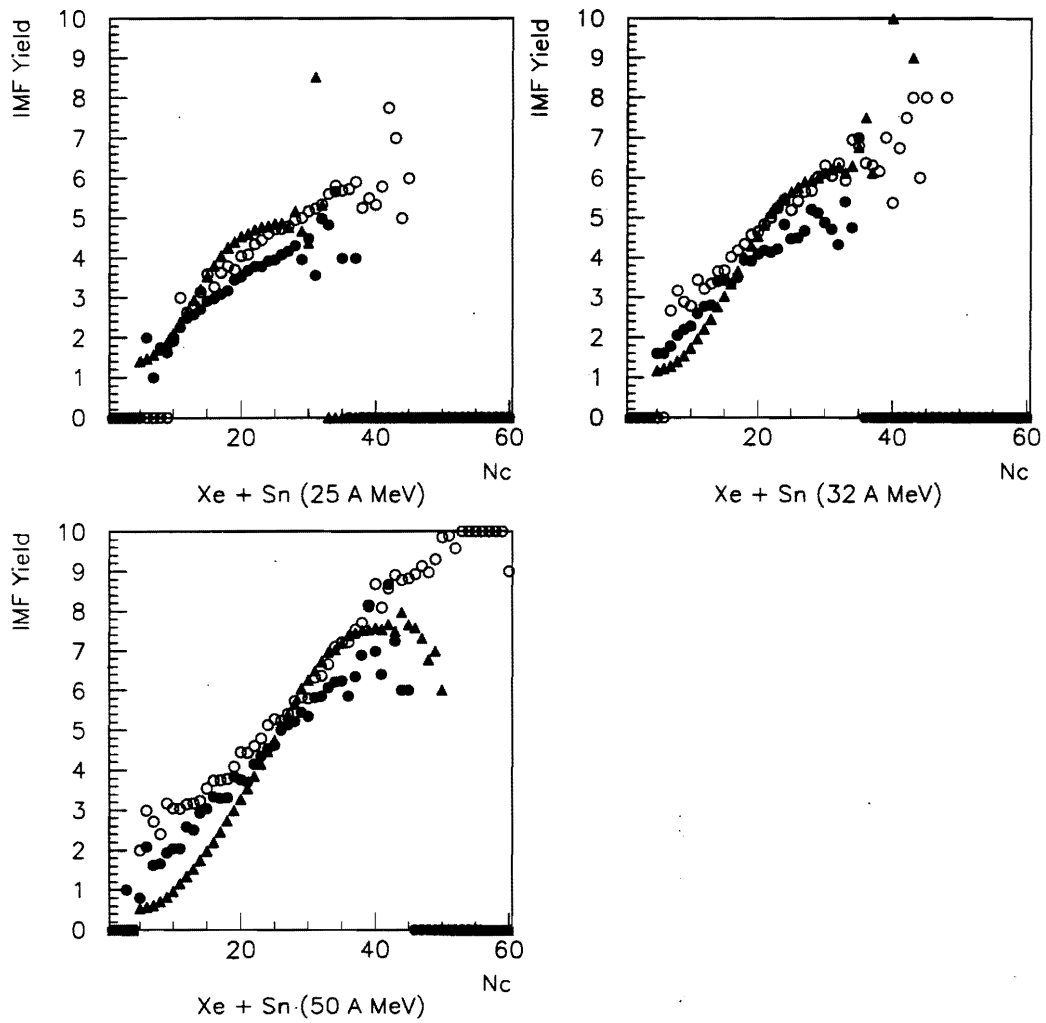

Figure 3: Mean fragment multiplicity as a function of the number of charged particle N_C for Xe+ Sn at three different energies. We compare the experiment with the filtered Q.M.D. results.

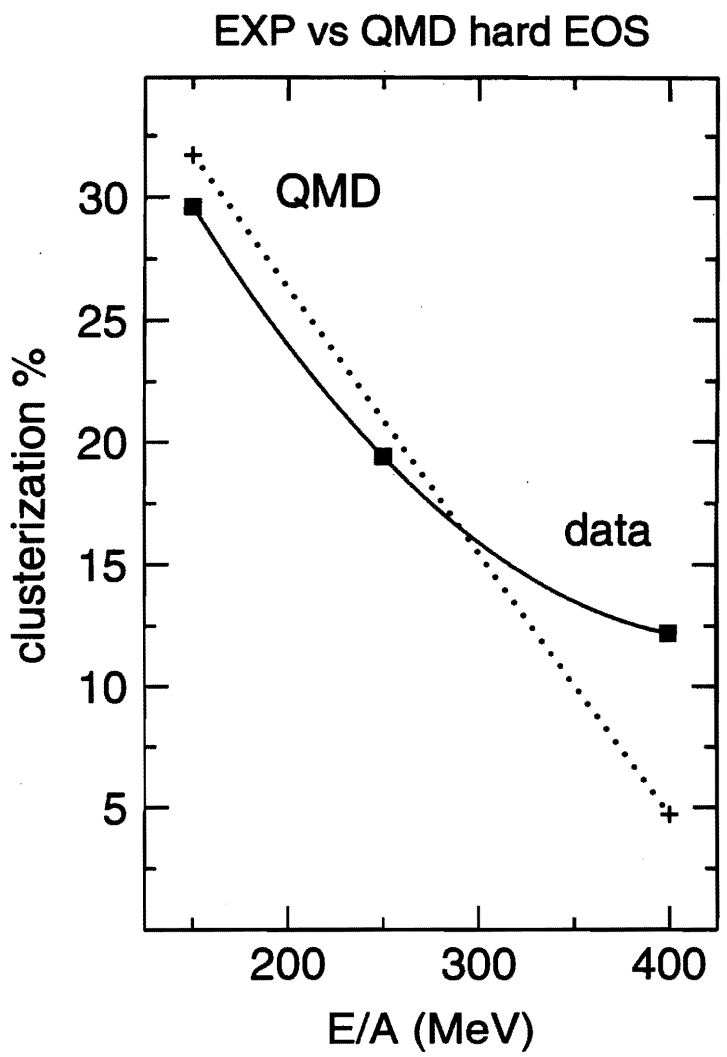

zclust.data

Figure 4: Percentage of nucleons bound in clusters as a function of the beam energy as calculated with Q.M.D. and compared to the FOPI experiments by the FOPI collaboration

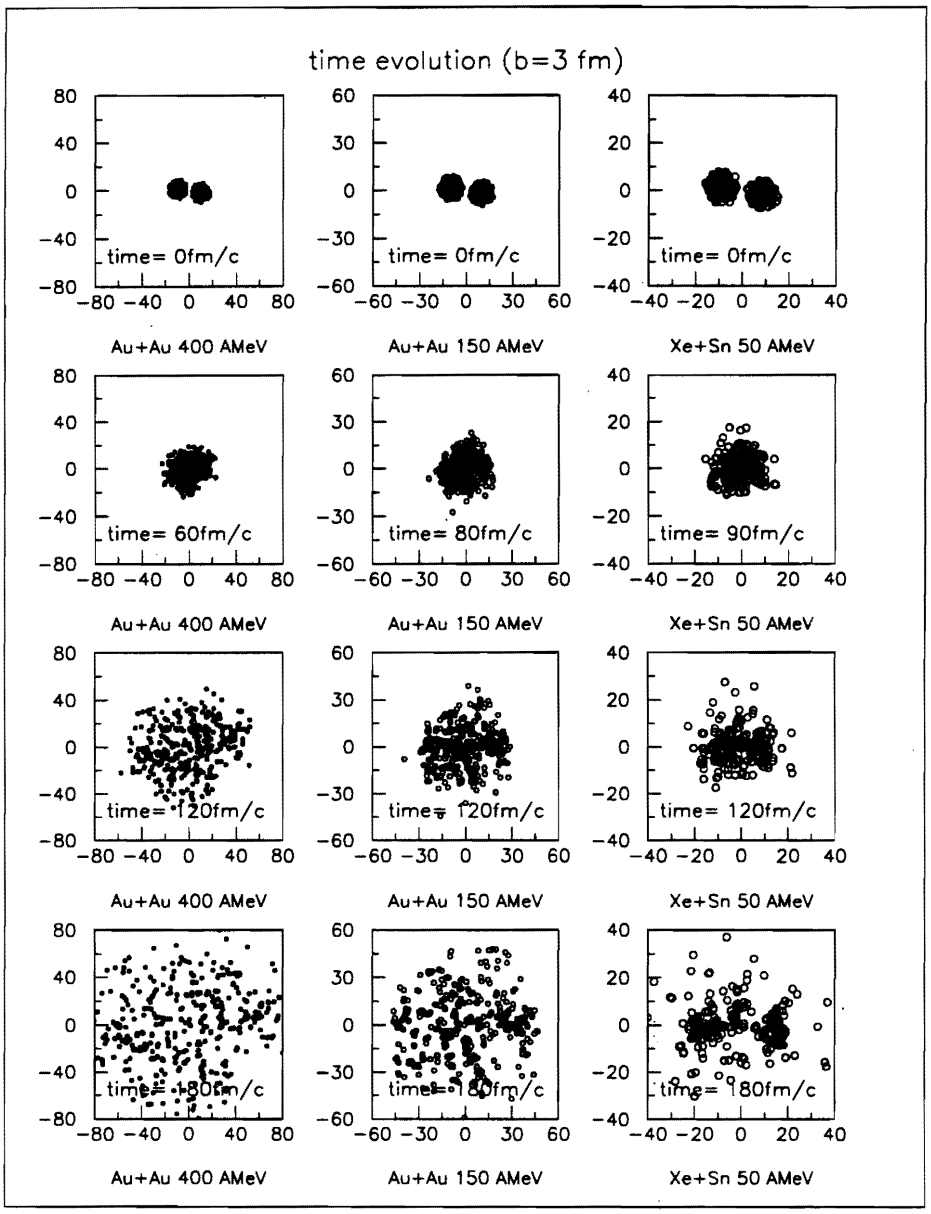

Figure 5: Time evolution of three central reactions

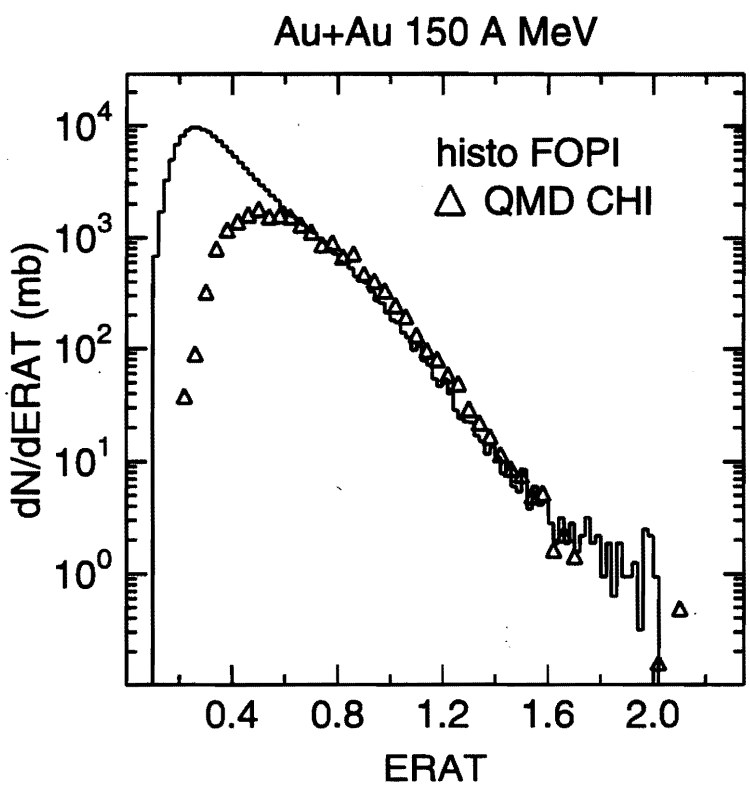

erats.data

Figure 6: $dN/dErat$ of filtered Q.M.D. simulations as compared to the FOPI experiment

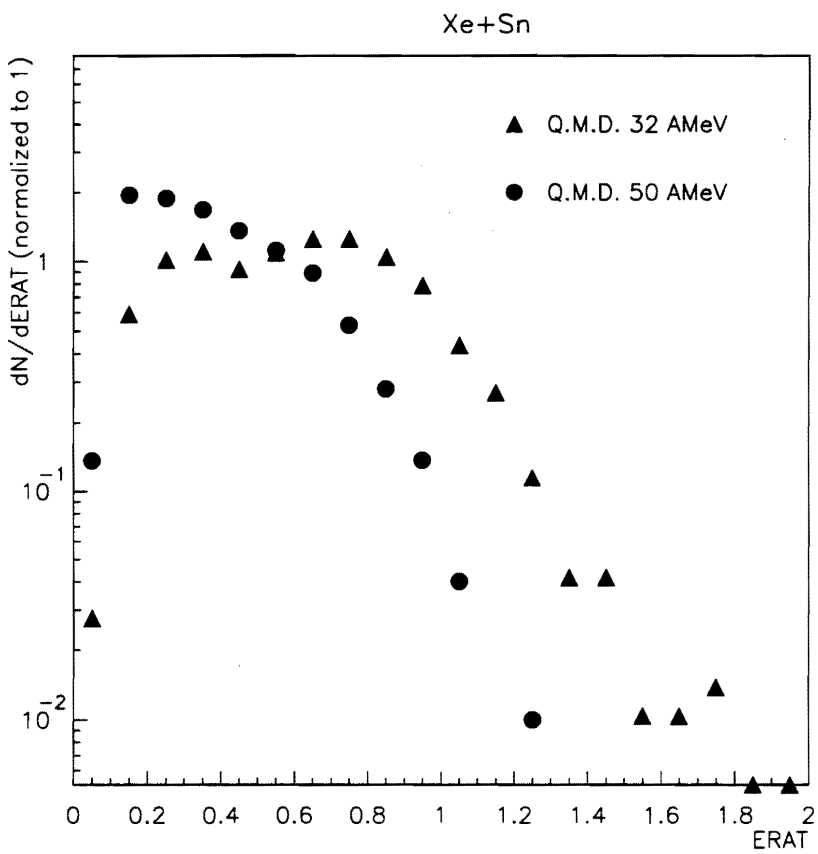

Figure 7: $dN/dErat$ **for the Xe + Sn at 32 and 50 AMeV**

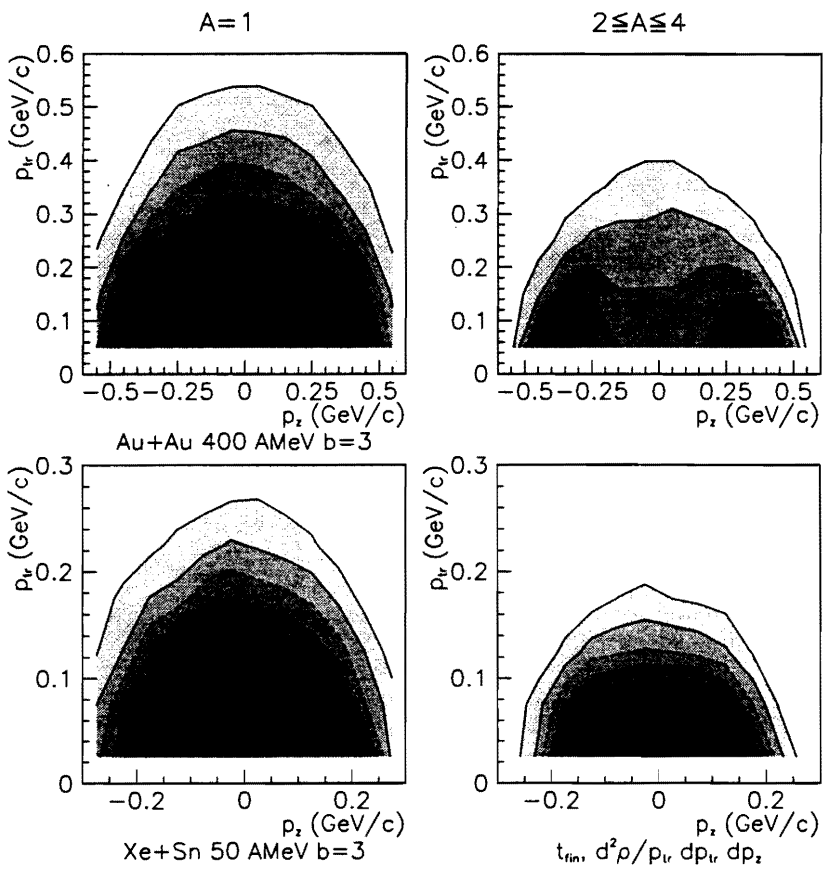

Figure 8: $d\sigma/p_t\,dp_t\,dp_z$ **for A + 1 and** $2 \leq A \leq 4$ **for Au + Au at 400 AMeV and Xe + Sn at 50 AMeV**

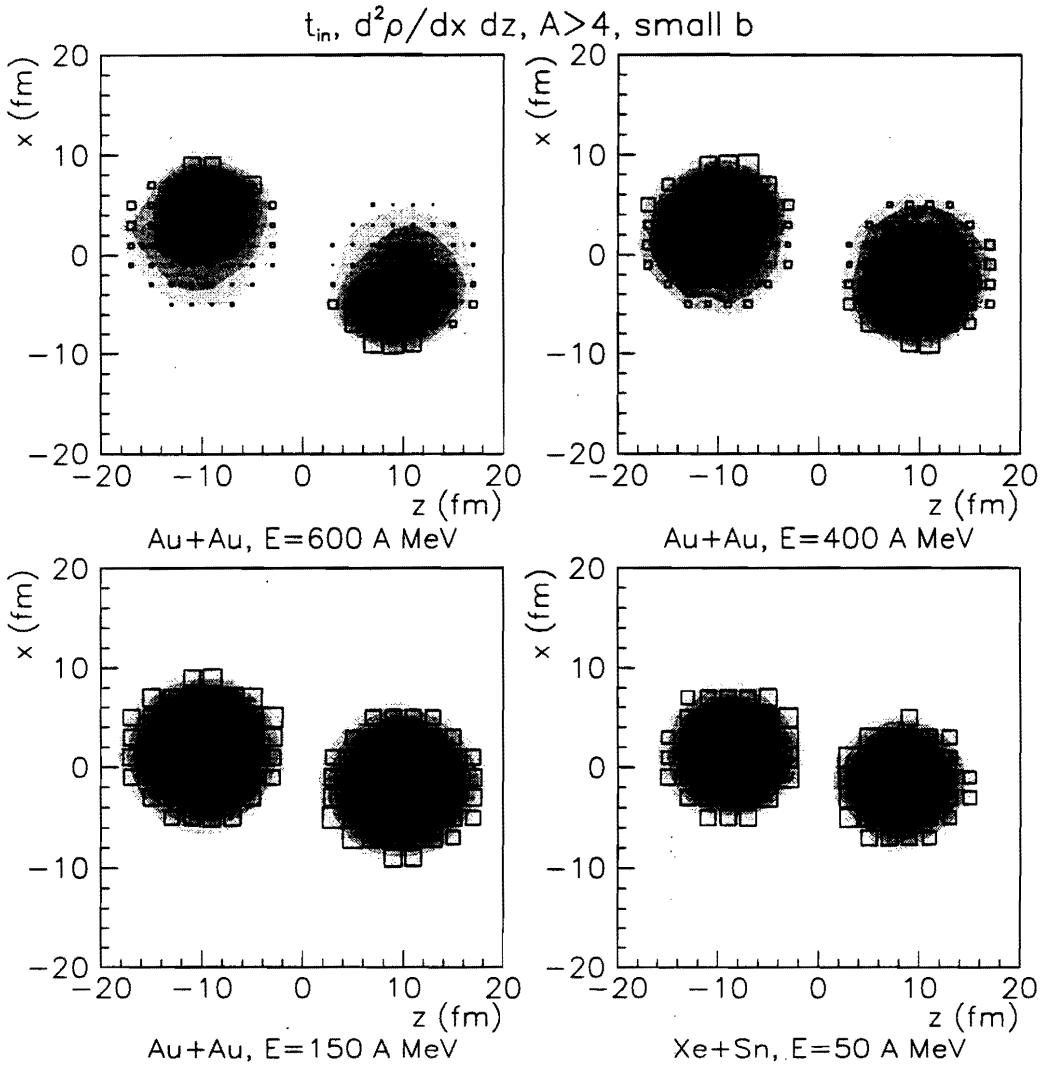

Figure 9: Coordinate space initial-final state correlation of nucleons entrained finally in heavy fragments for b = 3 fm

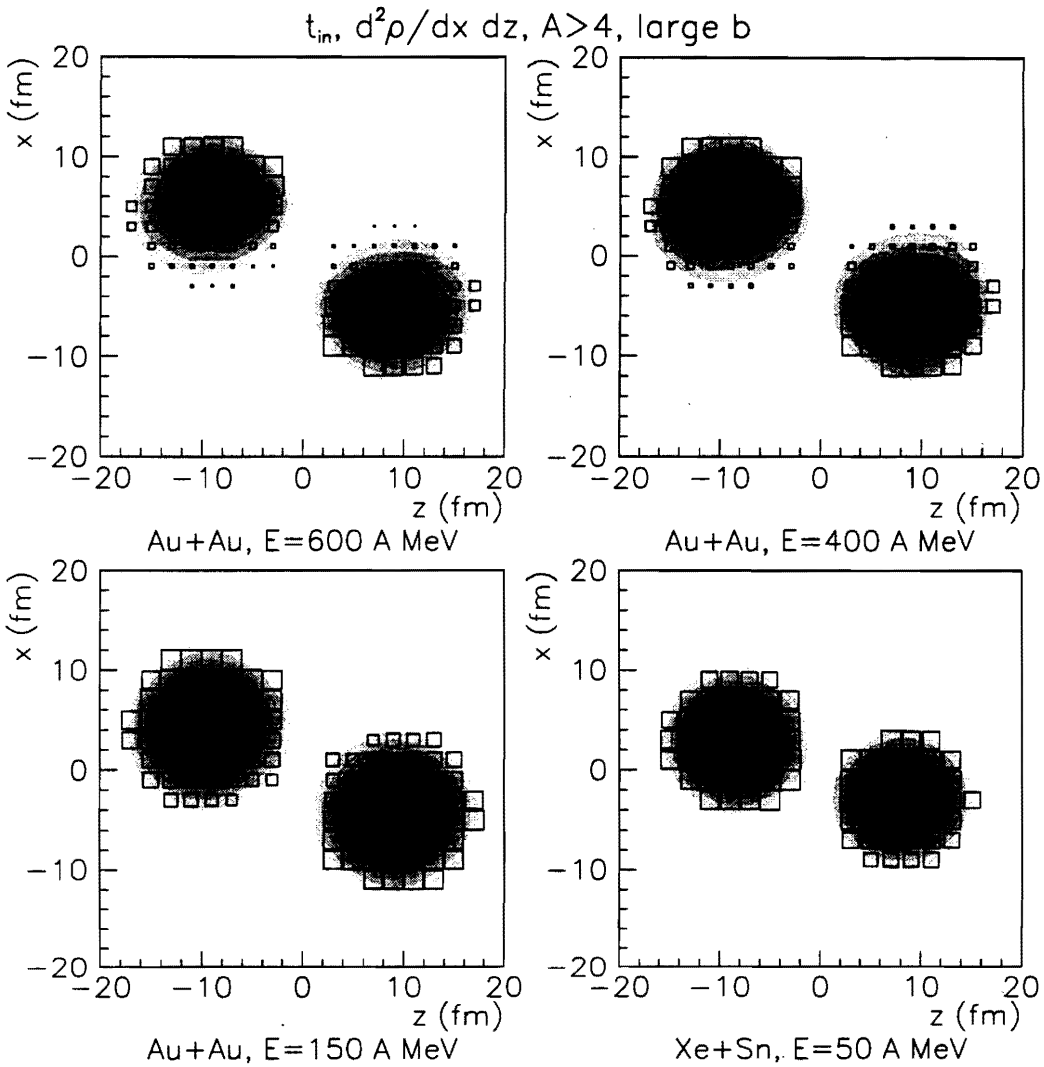

Figure 10: Coordinate space initial-final state correlation of nucleons entrained finally in heavy fragments for b = 6 resp. 8 fm

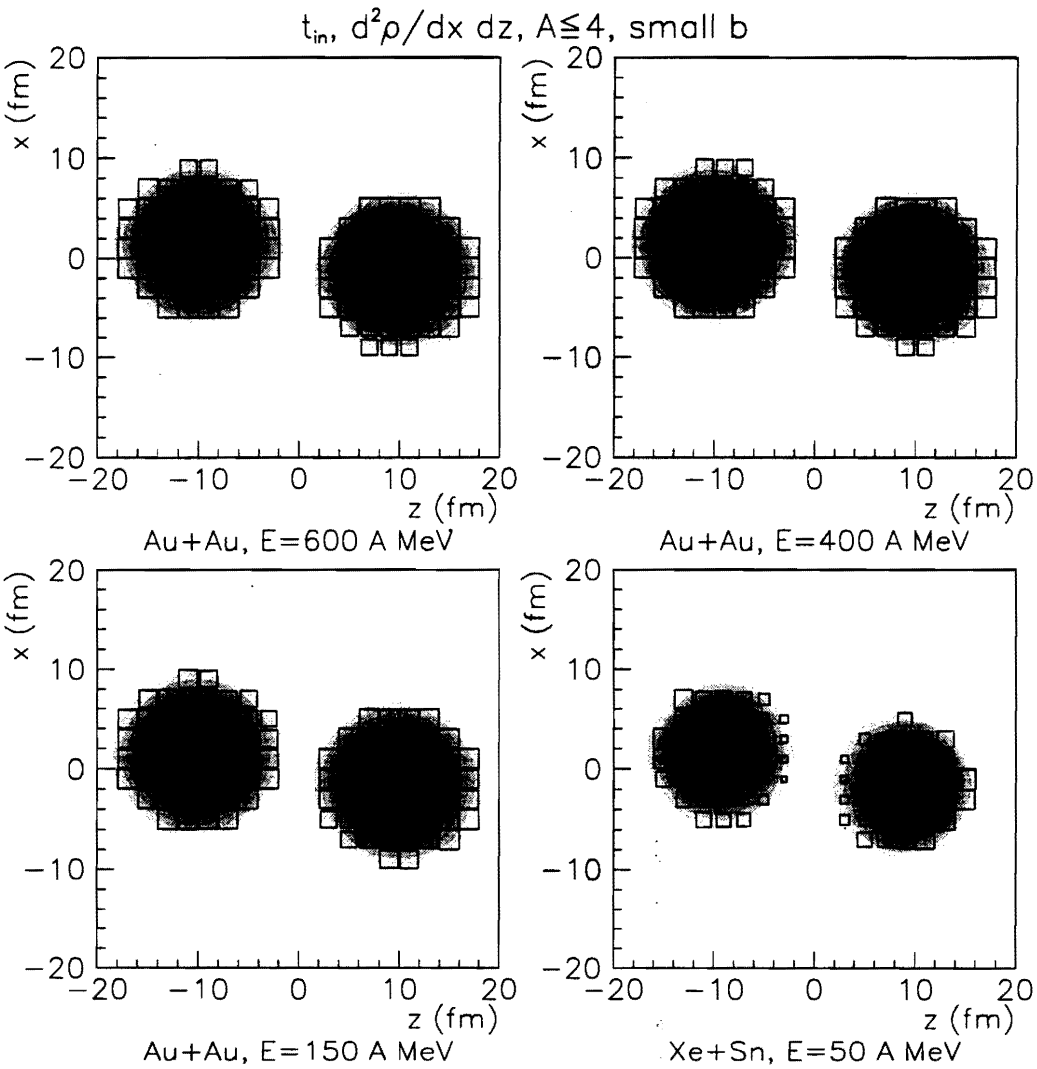

Figure 11: Coordinate space initial-final state correlation of nucleons entrained finally in light fragments or being singles for b = 3 fm

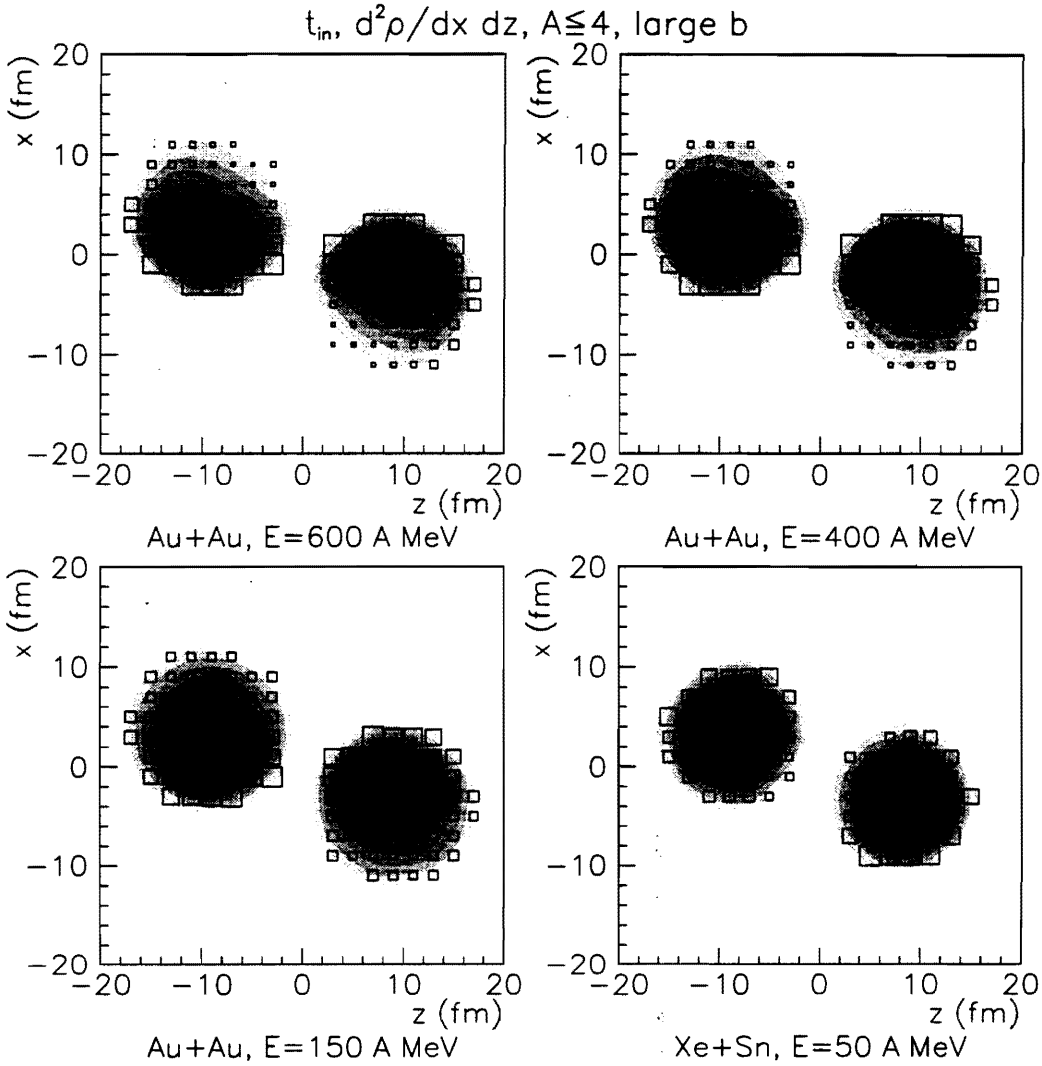

Figure 12: Coordinate space initial-final state correlation of nucleons entrained finally in light fragments or being singles for b = 6 resp. 8 fm

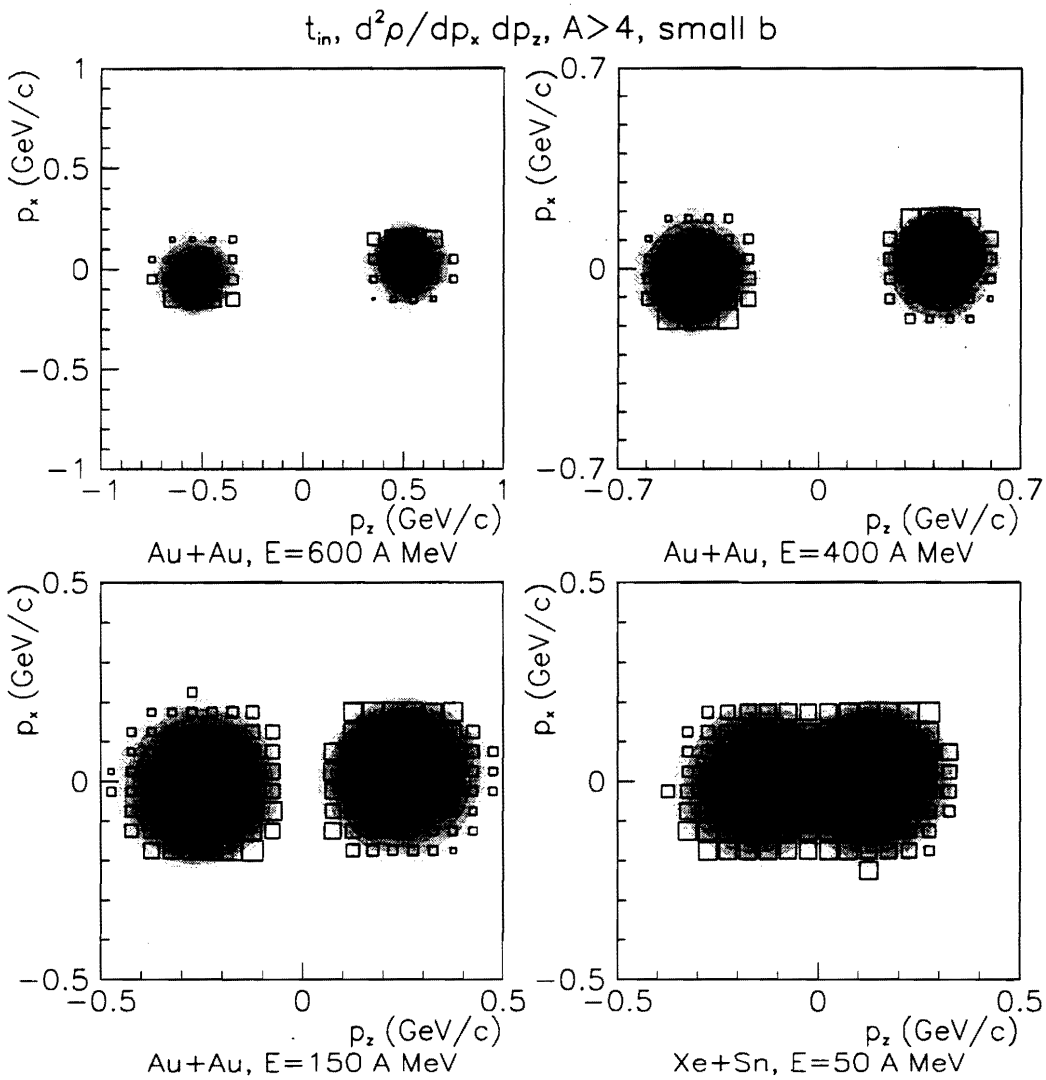

Figure 13: Momentum space initial-final state correlation of nucleons entrained finally in heavy fragments for b = 3 fm

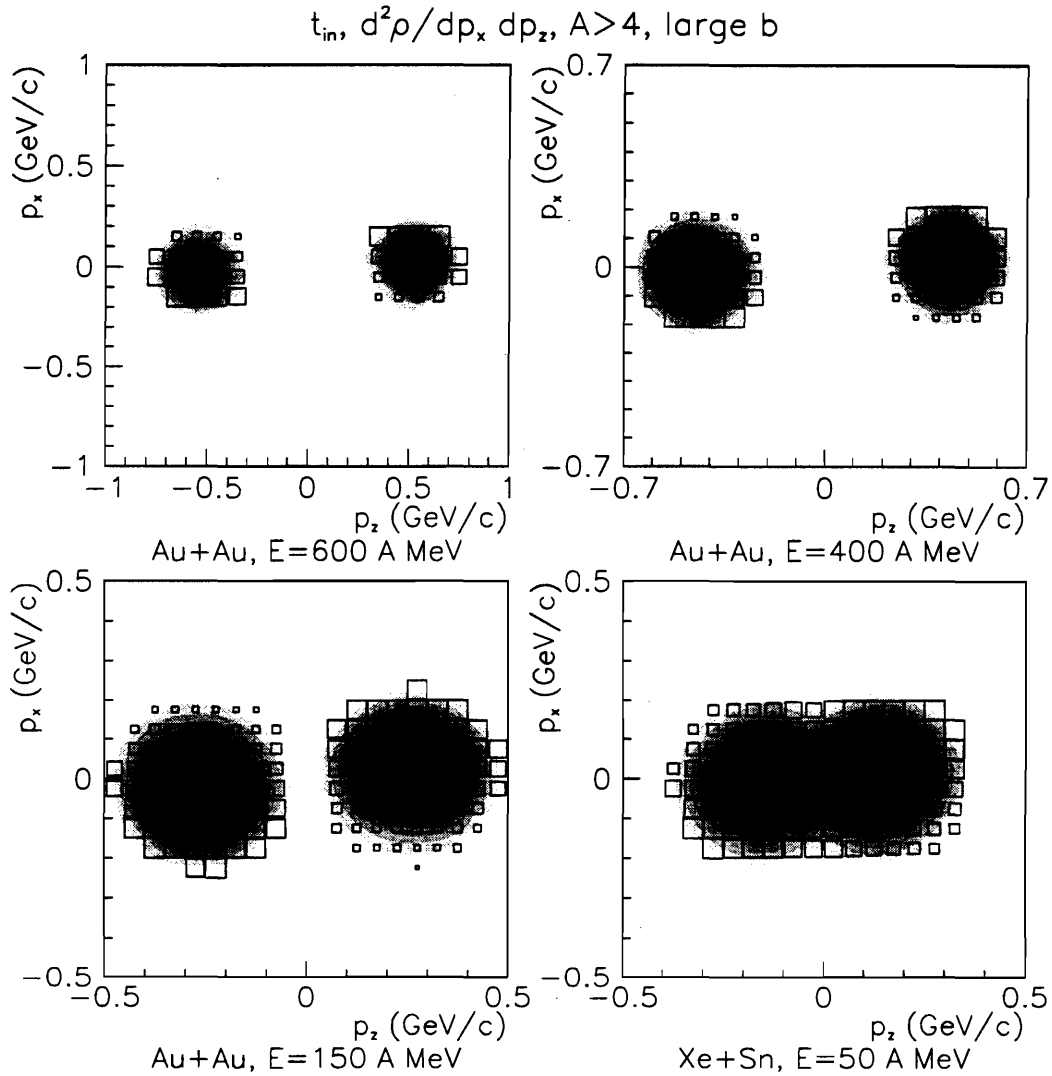

Figure 14: Momentum space initial-final state correlation of nucleons entrained finally in heavy fragments for b = 6 resp. 8 fm

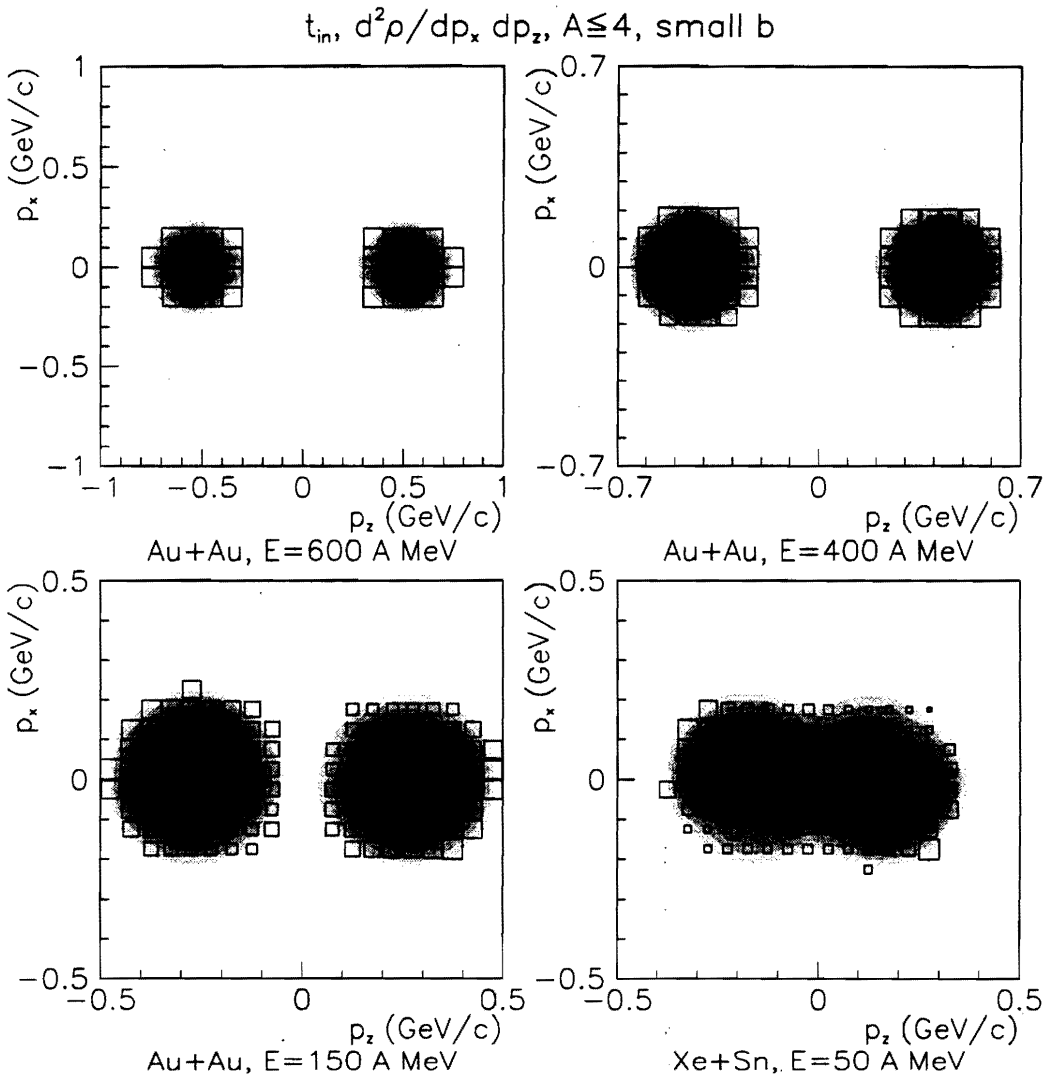

Figure 15: Momentum space initial-final state correlation of nucleons entrained finally in light fragments or being singles for b = 3 fm

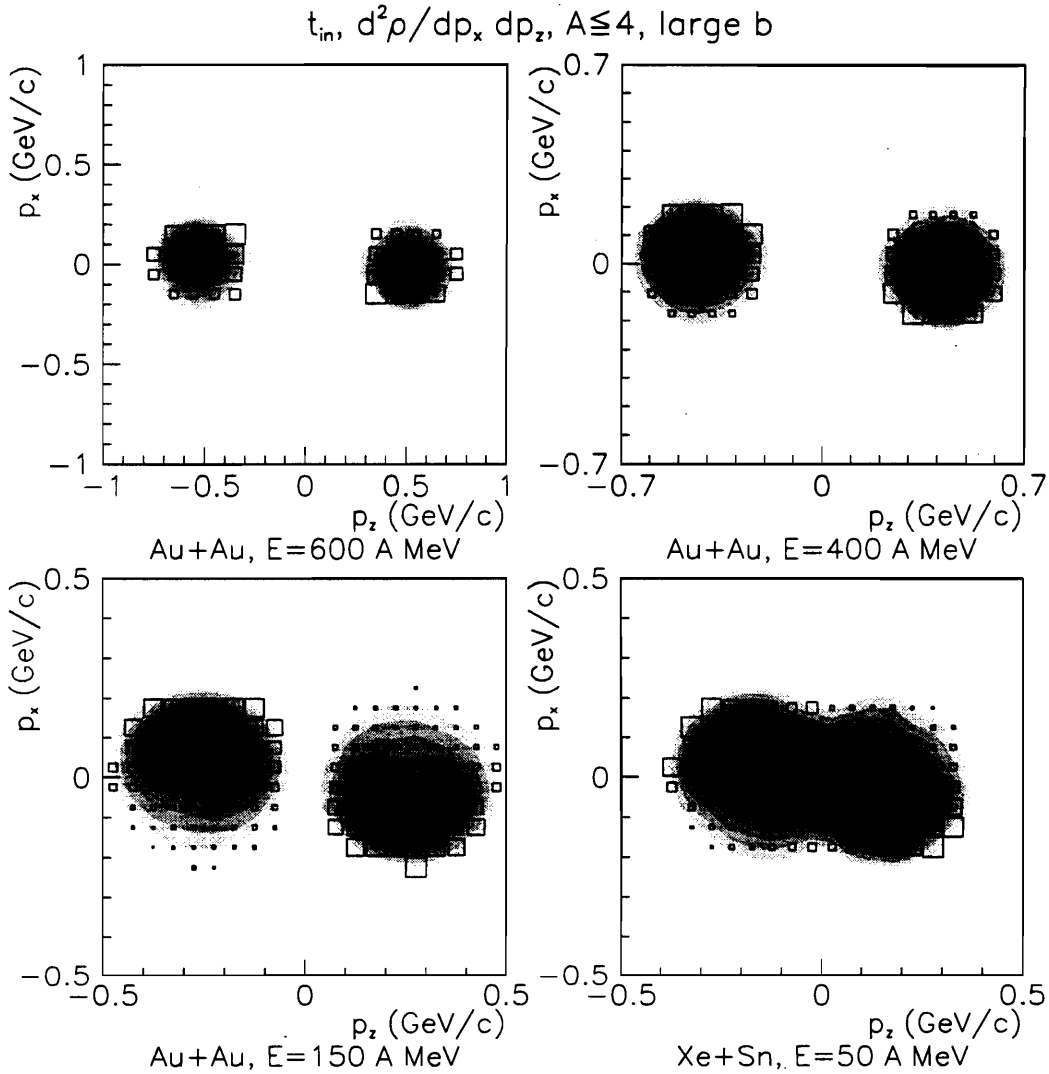

Figure 16: Momentum space initial-final state correlation of nucleons entrained finally in light fragments or being singles for b = 6 resp. 8 fm

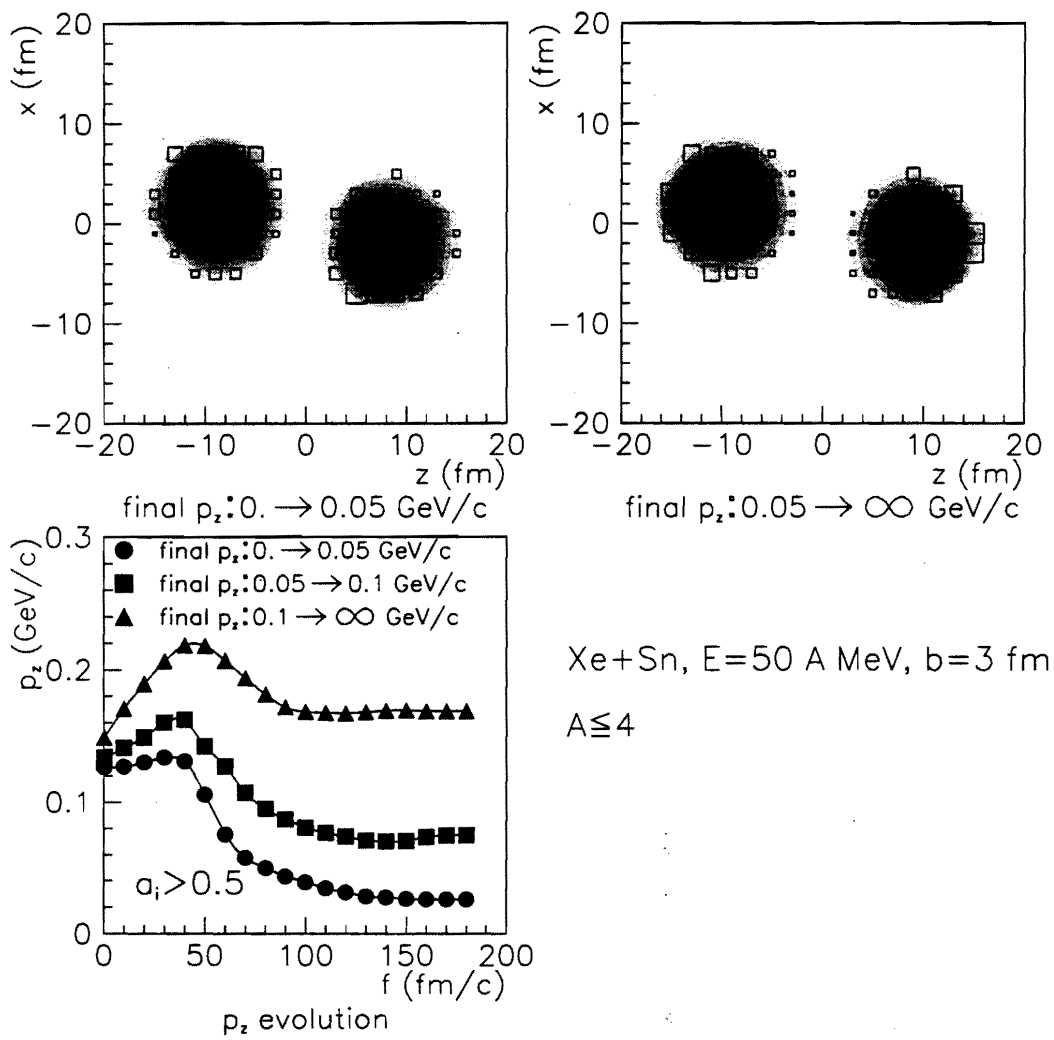

Figure 17: Initial position of those nucleons which are finally emitted with a small resp. a large longitudinal momentum in the reaction Xe + Sn at 50 A MeV. We display as well the time evolution of the longitudinal momentum for three classes of nucleons

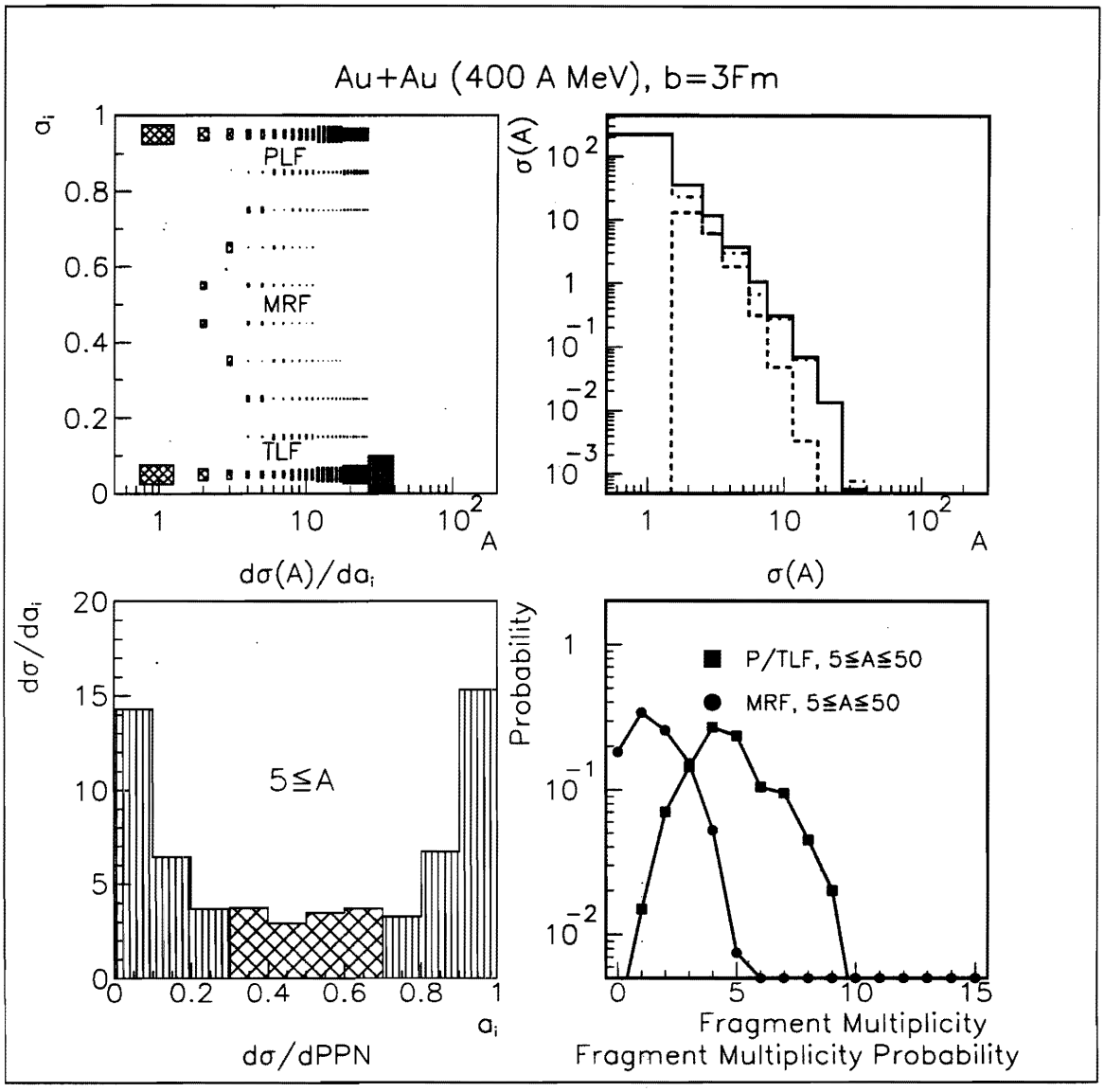

Figure 18: P/TLF and MRF for Au+Au, 400 AMeV, b = 3 fm On the right hand side we display the mass yield of P/TLF (full) and MRF (dashed) as well as the multiplicity distribution, on the left hand side the composition of the fragments

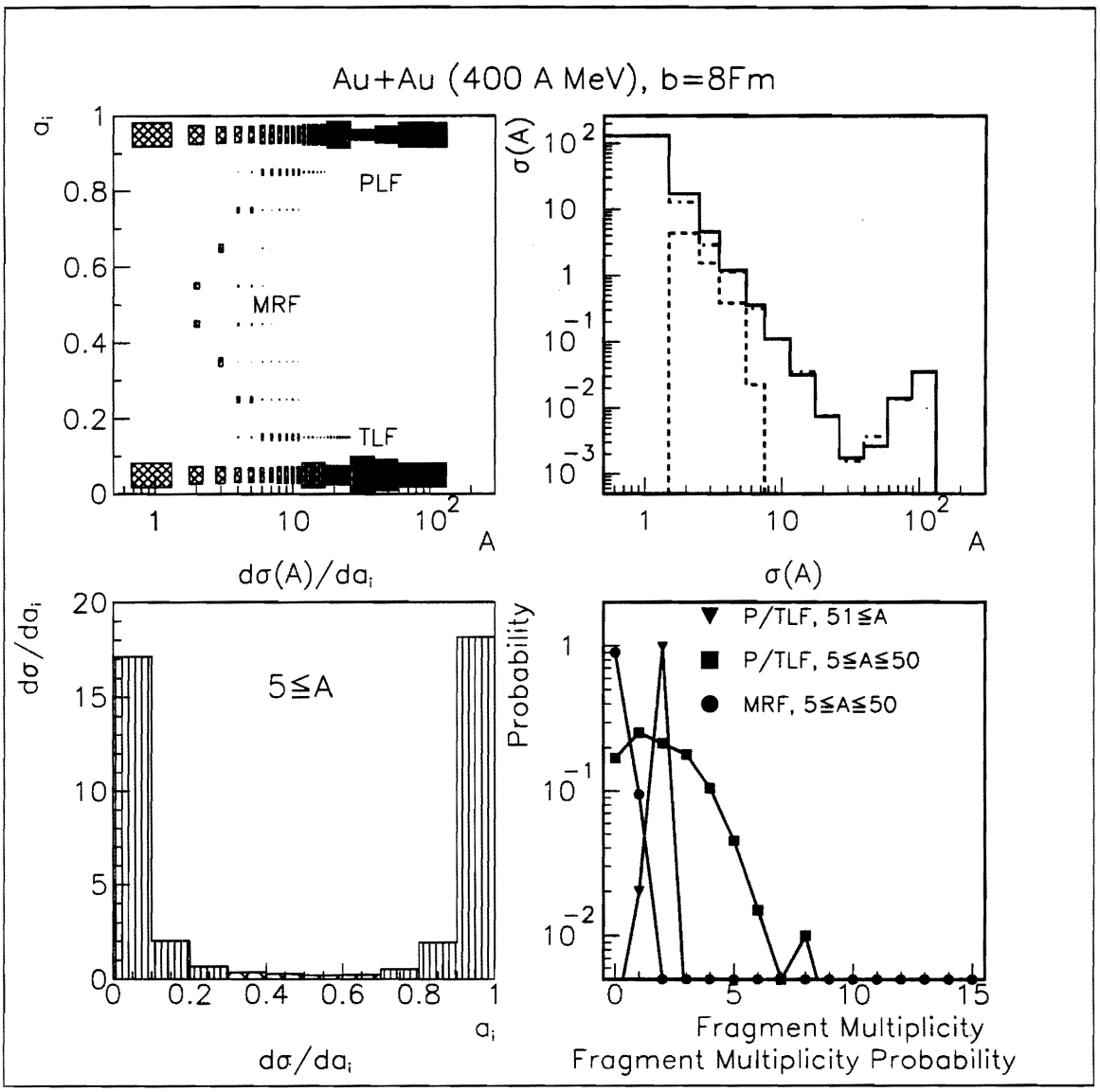

Figure 19: P/TLF and MRF for Au+Au, 400 AMeV, b = 8 fm On the right hand side we display the mass yield of P/TLF (full) and MRF (dashed) as well as the multiplicity distribution, on the left hand side the composition of the fragments

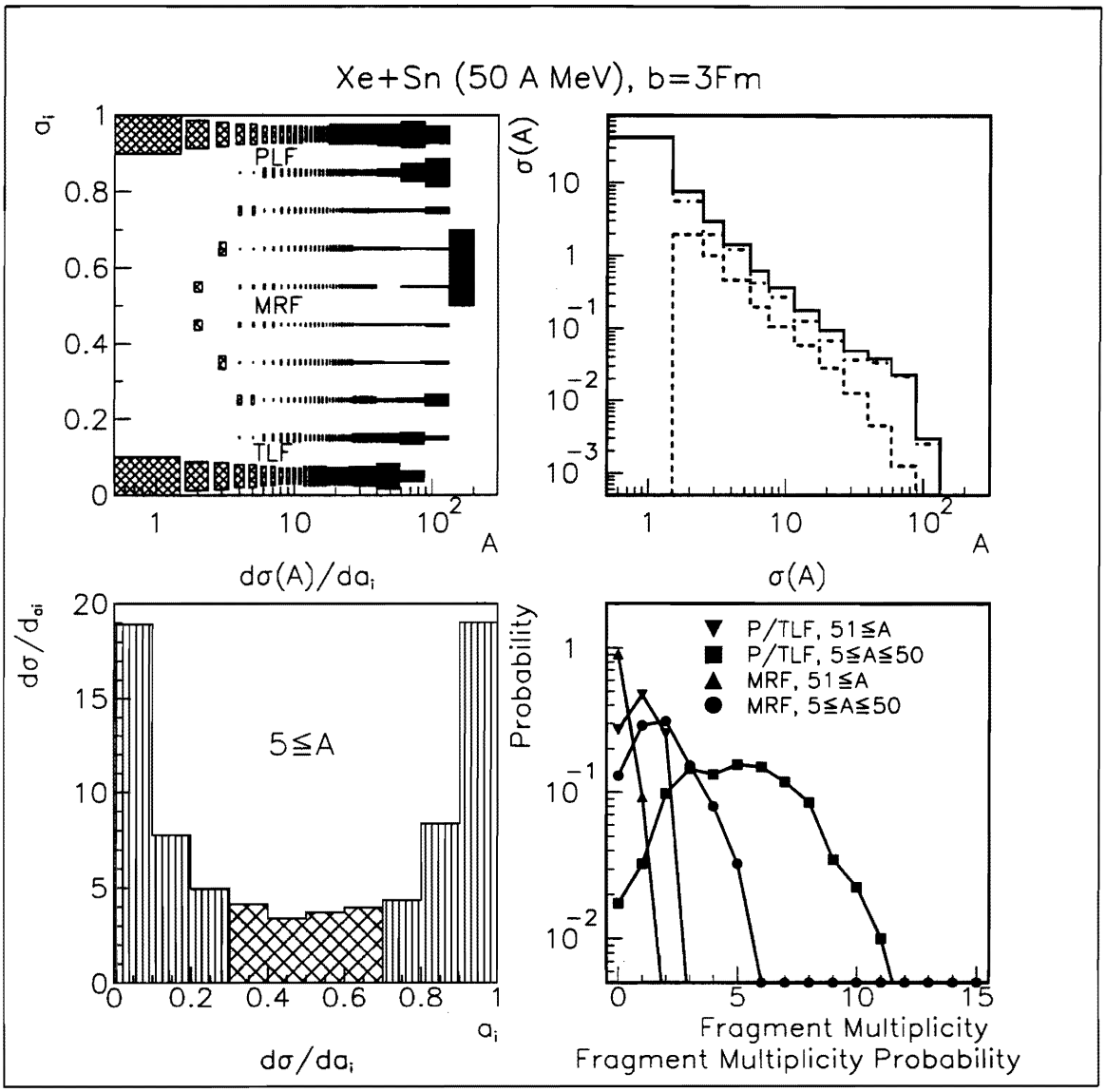

Figure 20: P/TLF and MRF for Xe+Sn, 50 AMeV, b = 3 fm On the right hand side we display the mass yield of P/TLF (full) and MRF (dashed) as well as the multiplicity distribution on the left hand side the composition of the fragments

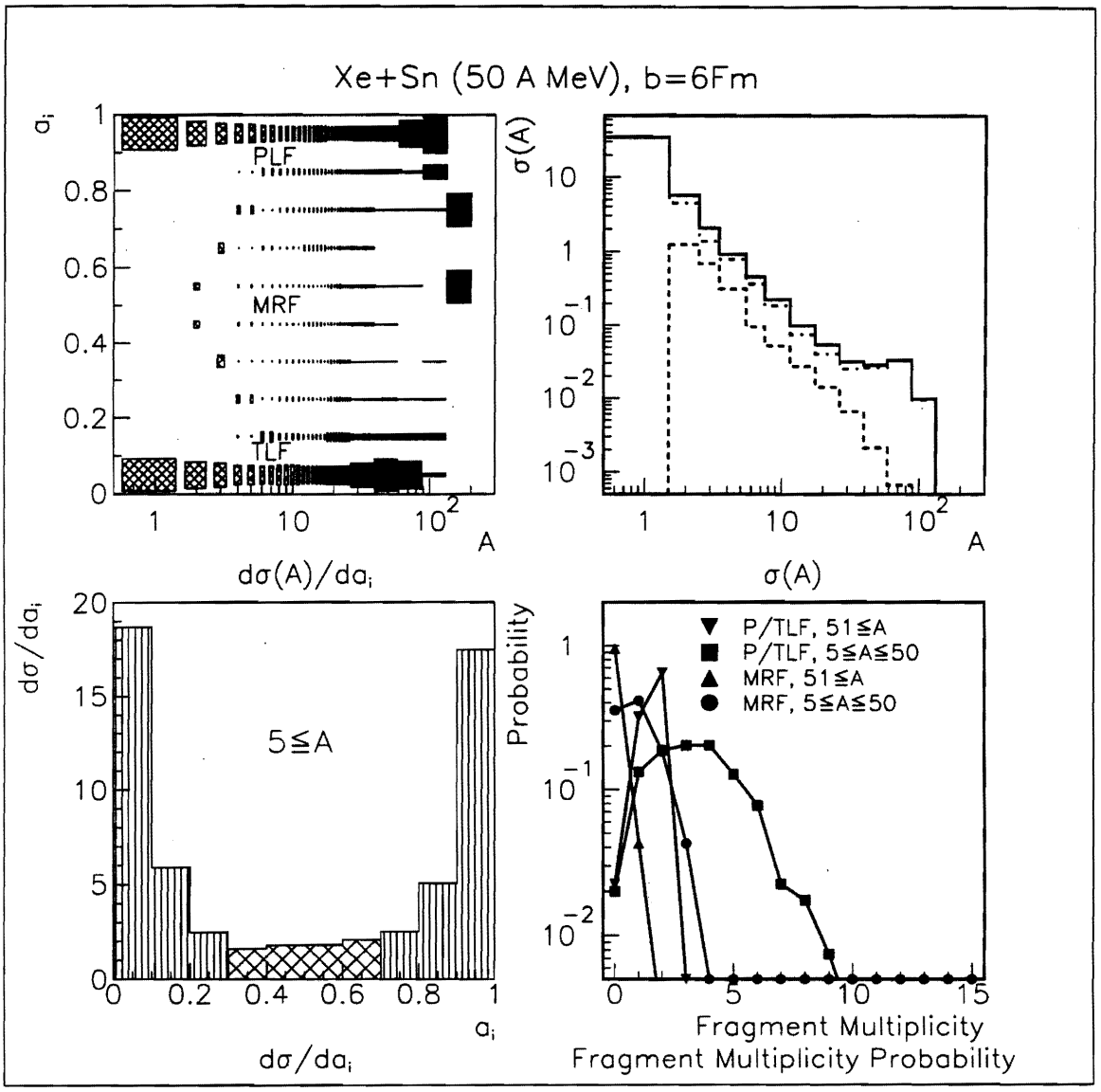

Figure 21: P/TLF and MRF for Xe+Sn, 50 AMeV, b = 6 fm On the right hand side we display the mass yield of P/TLF (full) and MRF (dashed) as well as the multiplicity distribution on the left hand side the composition of the fragments

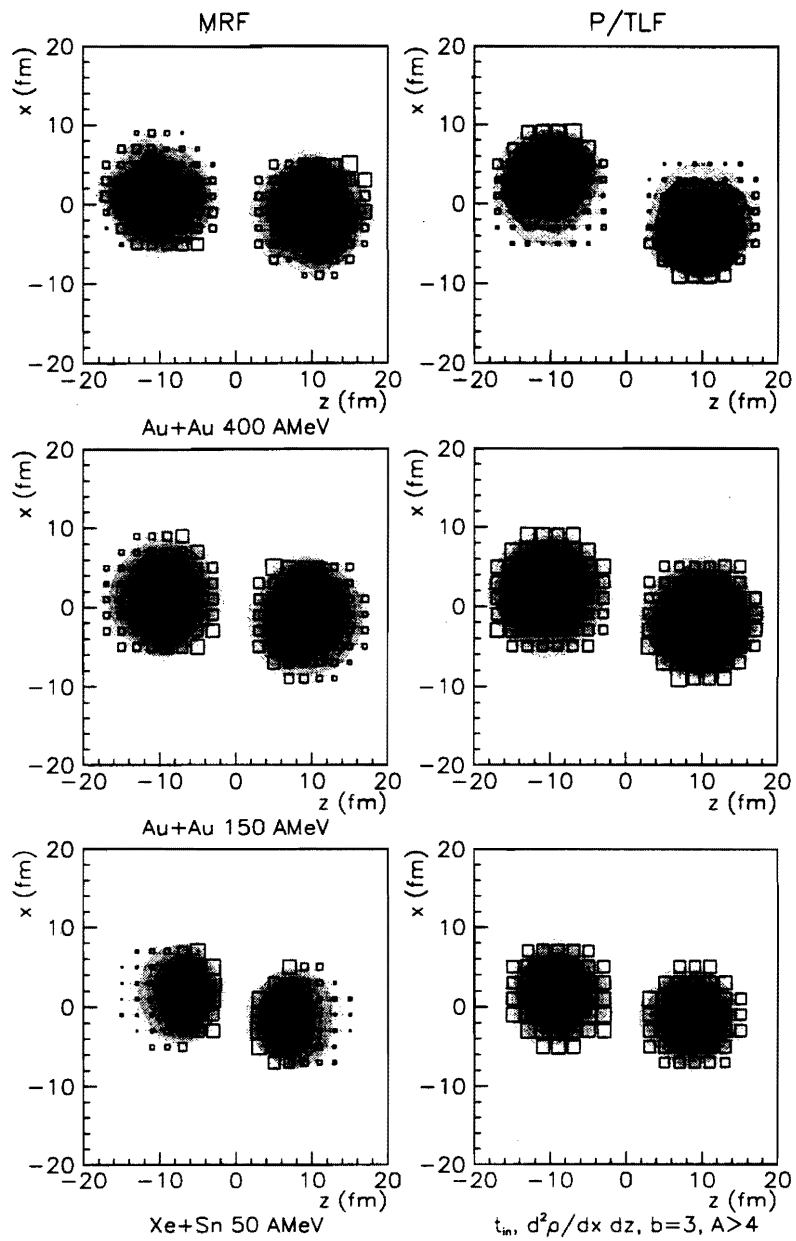

Figure 22: Coordinate space initial-final state correlation of nucleons entrained finally in heavy fragments for b = 3 fm, separately for MRF's and P/TLF's

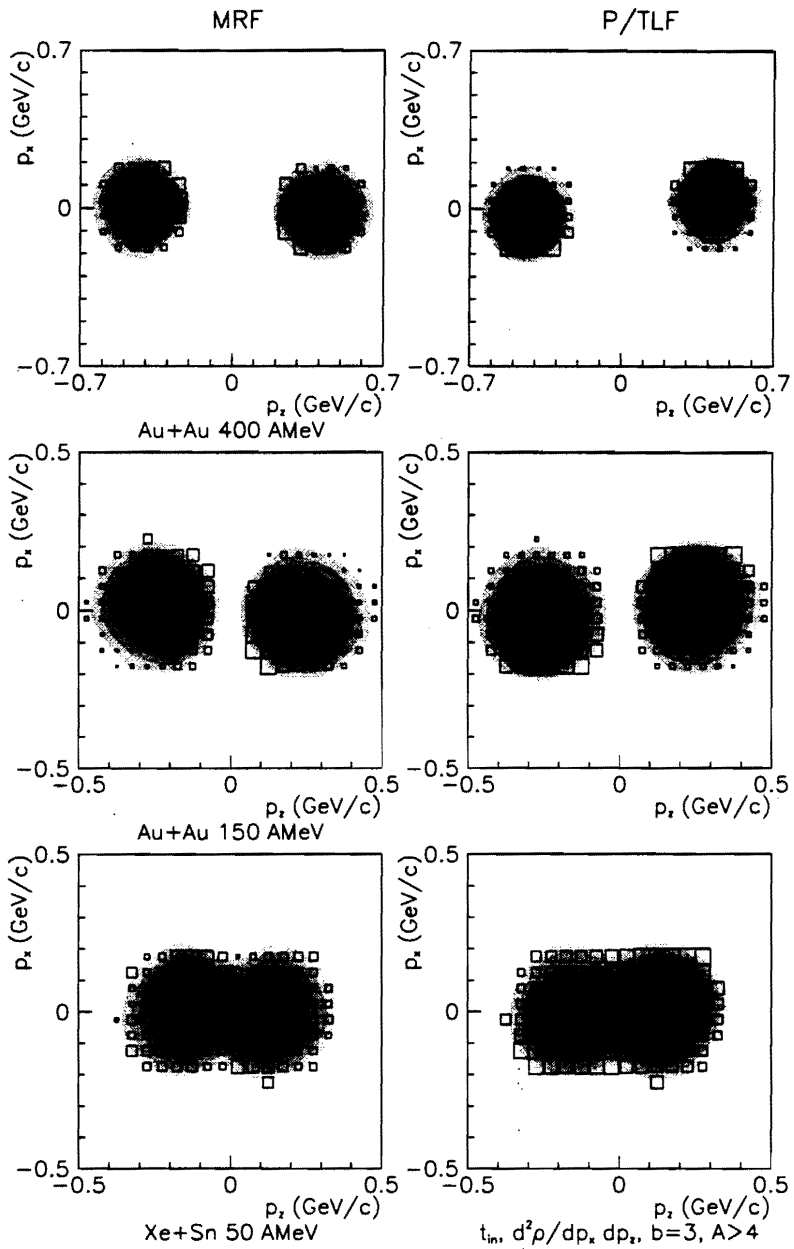

Figure 23: Momentum space initial-final state correlation of nucleons entrained finally in heavy fragments for b = 3 fm, separately for MRF's and P/TLF's

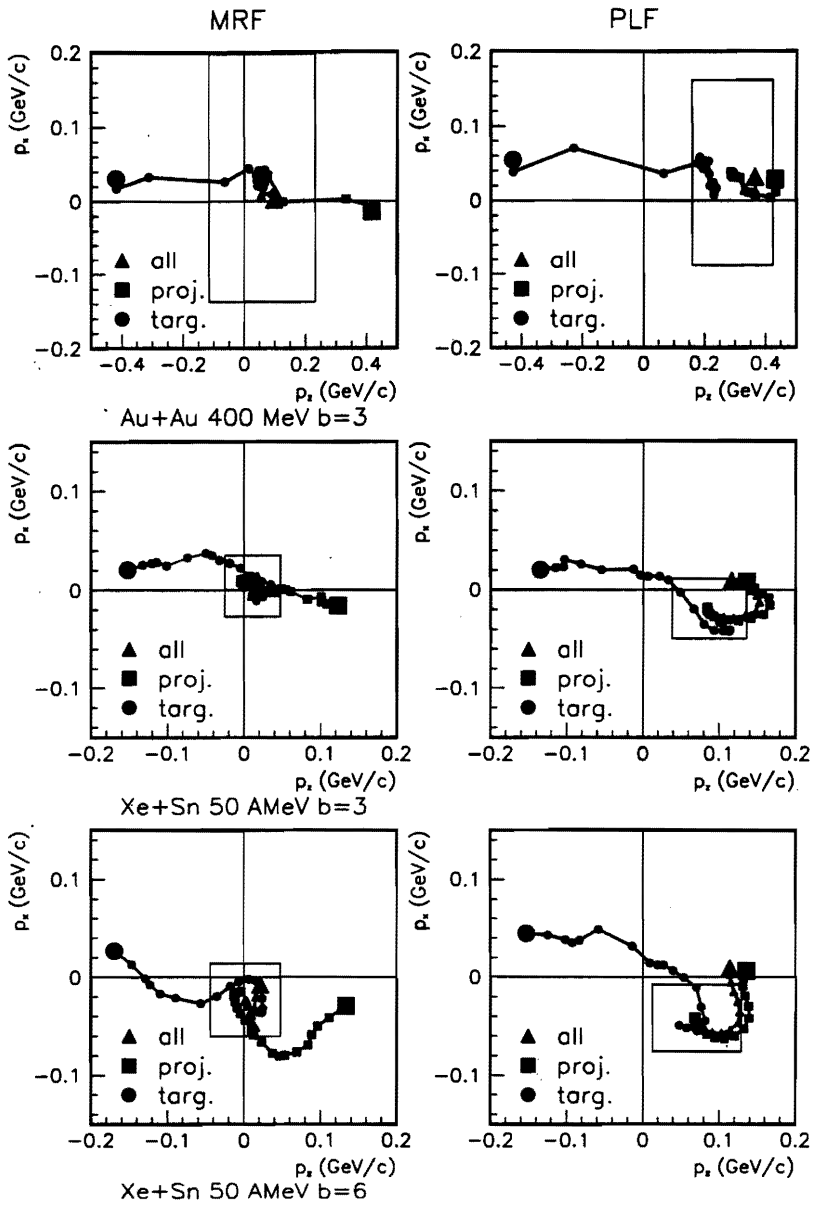

Figure 24: Trajectories in momentum space for three of the investigated reactions. The initial value is marked by an enlarged symbol then the value has been plotted in time steps of 10 fm/c. The box gives the variance of the final value of "all".

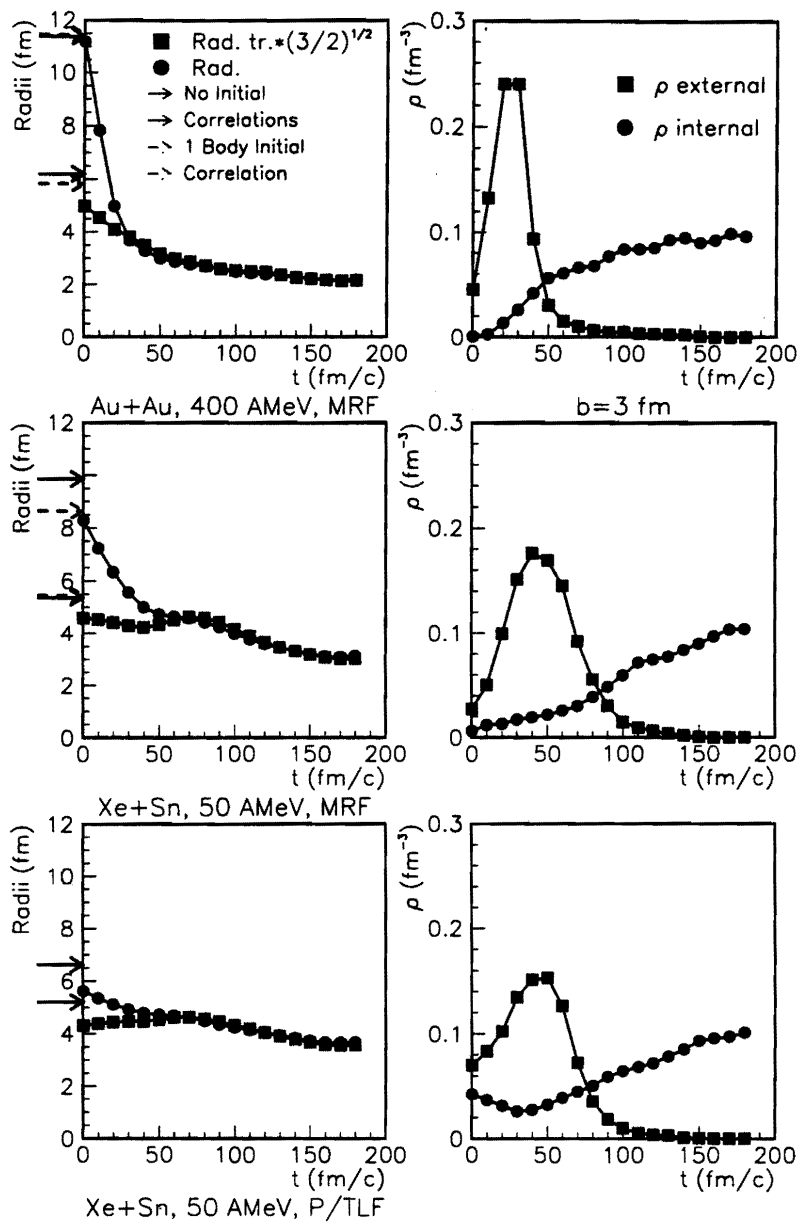

Figure 25: Time evolution of the radii (transverse and total) and densities (external and internal) for the b = 3 fm reactions

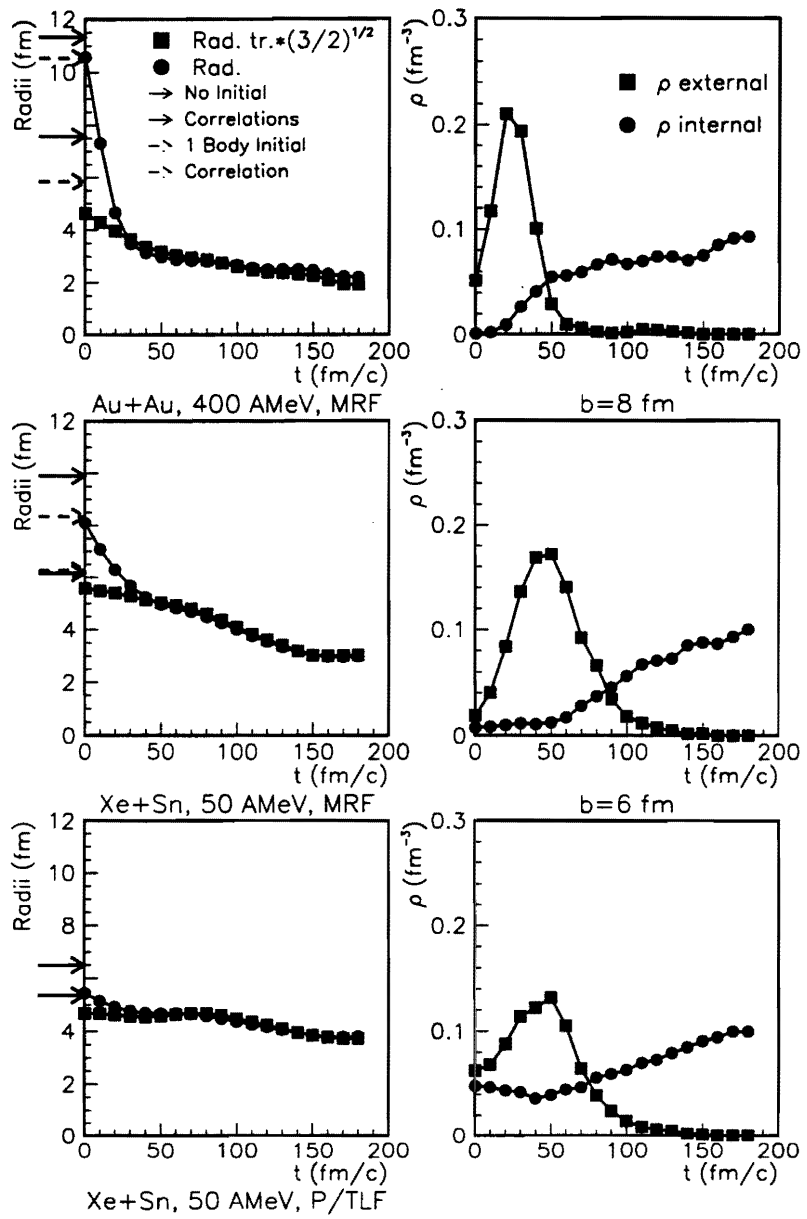

Figure 26: Time evolution of the radii (transverse and total) and densities (external and internal) for the b = 6 resp. 8 fm reactions

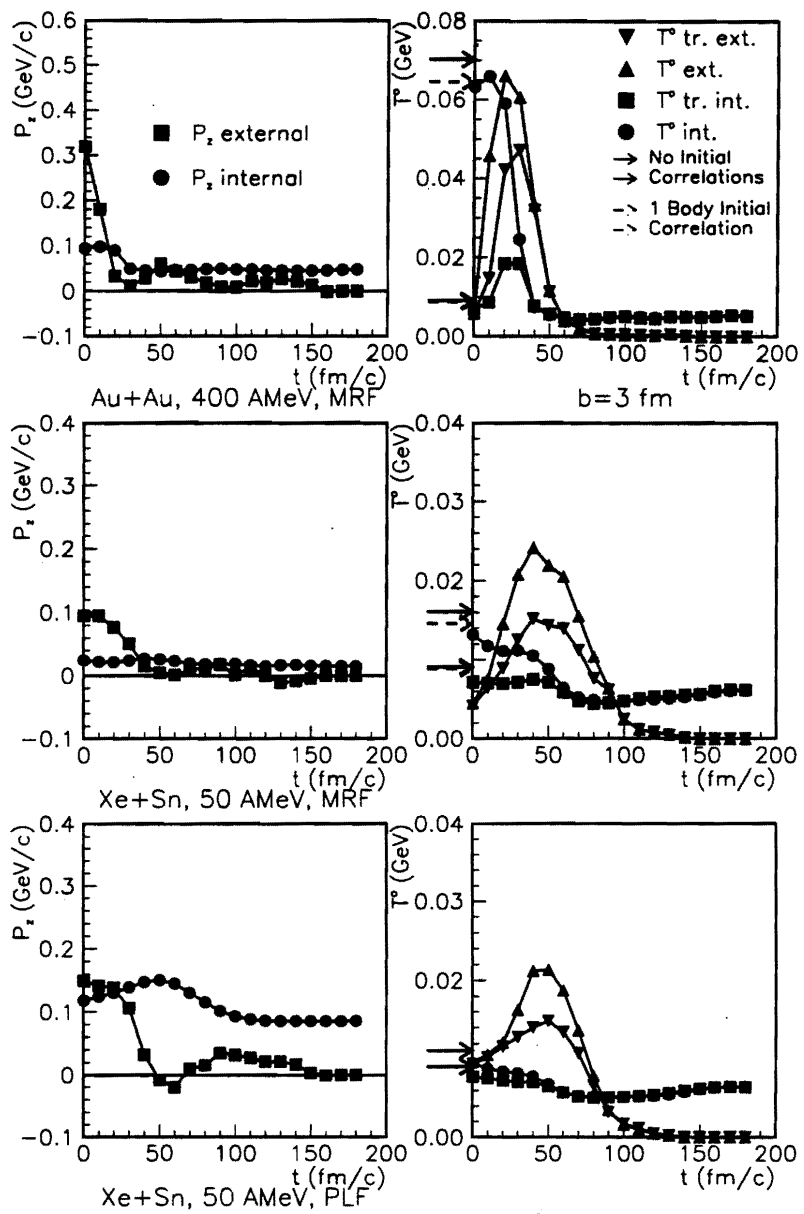

Figure 27: Time evolution of the longitudinal momentum (external and internal) and temperatures (external and internal, transversal and total) for the b = 3 fm reactions

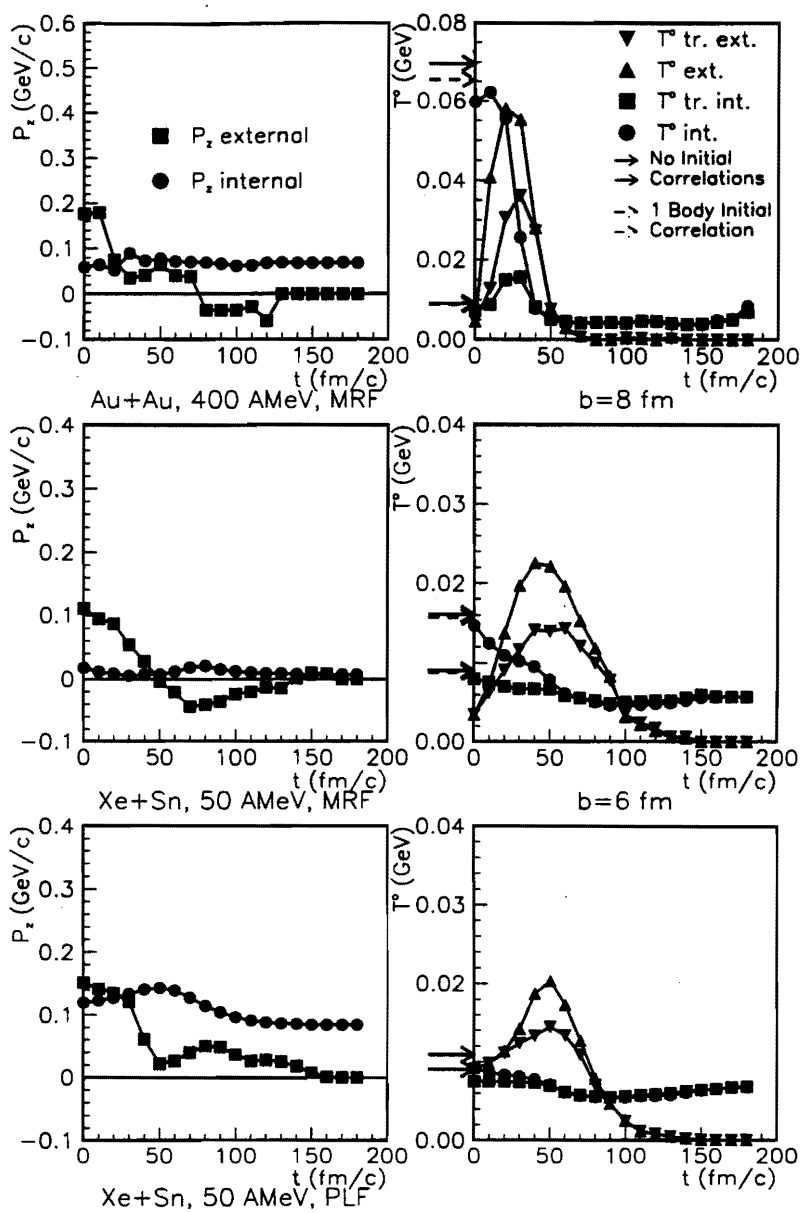

Figure 28: Time evolution of the longitudinal momentum (external and internal) and temperatures (external and internal, transversal and total) for the b = 6 resp. 8 fm reactions

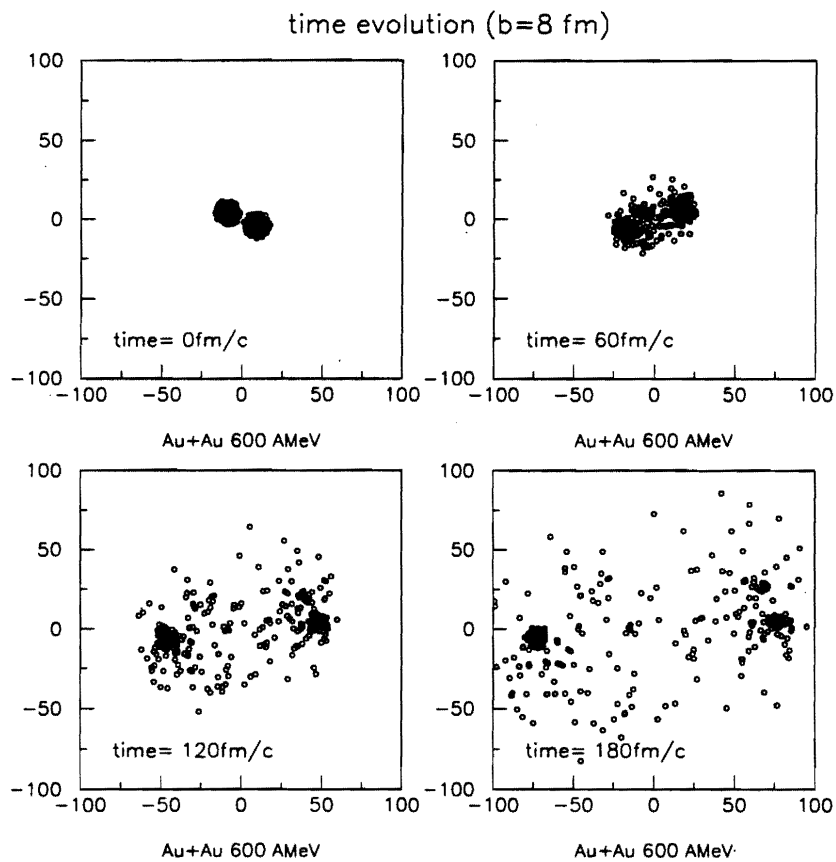

Figure 29: Scatter plot of a reaction b= 8 fm 600 A MeV Au + Au projected onto the reaction plane

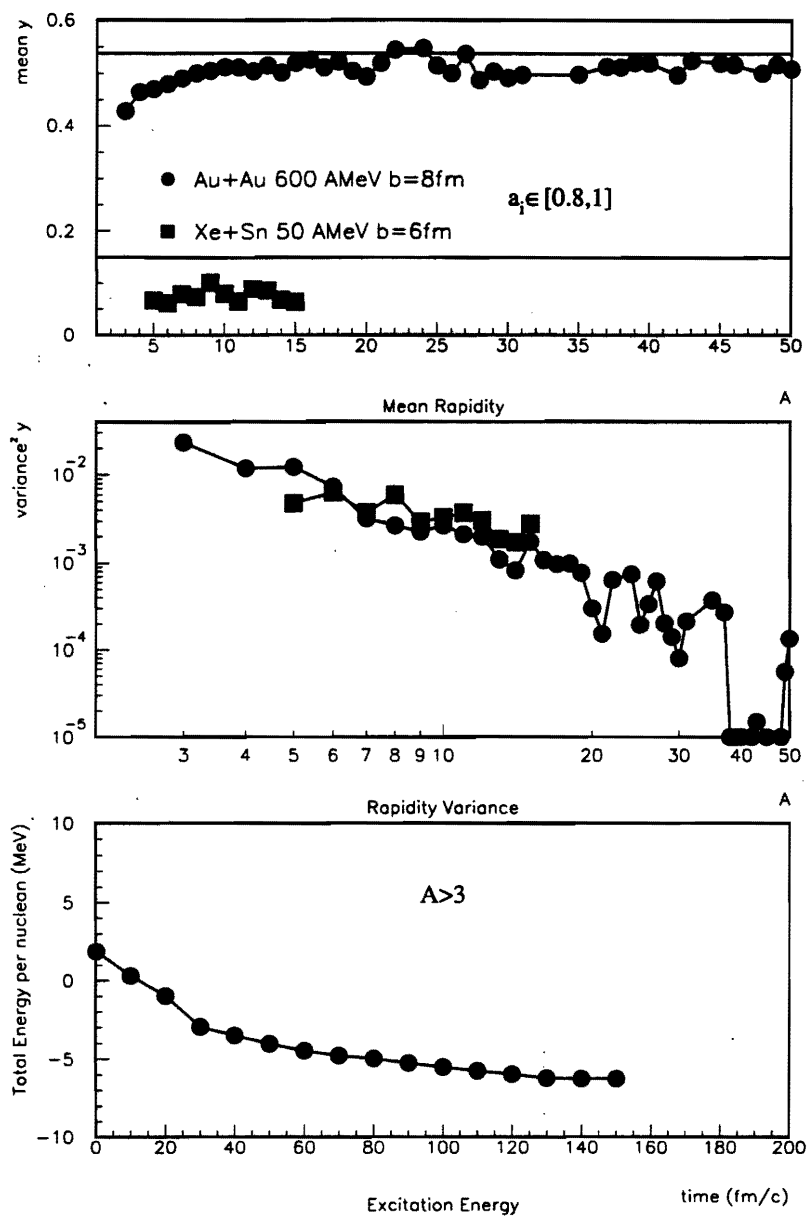

Figure 30: Mean rapidity and variance ^{2} of the rapidity distribution for fragments produced in the reaction 600 A MeV Au + Au, b = 8 fm. The bottom row displays the total energy per nucleons averaged over all spectator like fragments with $A > 3$.